

## NASA Technical Paper 1673

LOAN COPY: RI  
AFWL TECHNIC  
KIRTLAND AFB

0067740



TECH LIBRARY KAFB, NM

# Pollutant Emissions From Flat-Flame Burners at High Pressures

Howard G. Maahs and Irvin M. Miller

JUNE 1980

21

**NASA**



0067740

NASA Technical Paper 1673

# Pollutant Emissions From Flat-Flame Burners at High Pressures

Howard G. Maahs and Irvin M. Miller  
*Langley Research Center*  
*Hampton, Virginia*



National Aeronautics  
and Space Administration

**Scientific and Technical  
Information Office**

1980

## SUMMARY

Maximum flame temperatures and pollutant emission measurements for  $\text{NO}_x$ , CO, and UHC (unburned hydrocarbons) are reported for premixed methane-air flat flames at constant total mass flow rate over the pressure range from 1.9 to 30 atm and for equivalence ratios from 0.84 to 1.12. For any given pressure, maxima typically occur in both the temperature and  $\text{NO}_x$ -emissions curves slightly to the lean side of stoichiometric conditions. The CO emissions, however, increase continually with increasing equivalence ratio. Flame temperature and  $\text{NO}_x$  emissions decrease with increasing pressure, while the opposite is true for CO and UHC emissions. These changes are related, among other things, to the fact that heat transfer to the burner increases and residence time decreases as the pressure is increased.

Four flameholders, differing only slightly, were used in this study. In general, the temperature and emissions data from these four flameholders are similar, but some differences also exist. These differences appear to be related to minor variations in the condition of the flameholder surfaces. Since each flameholder has associated with it at least one set of anomalous emissions data, no one flameholder can be singled out as producing data most representative of an idealized flat flame. Because of this, attention should be focused primarily on the more general features of these temperature and emissions data; close attention to the finer details could lead to unwarranted conclusions because these are likely to be artifacts of the particular burners.

The  $\text{NO}_x$  data correlate reasonably well as a function of flame temperature only. These  $\text{NO}_x$  emissions are also believed to depend to some degree on pressure and equivalence ratio, but the true nature of these dependencies could not be firmly established from the present data.

## INTRODUCTION

In designing and modifying practical combustion devices (such as aircraft turbine engines, power plant combustors, internal combustion engines, etc.) for reduced pollutant emissions, detailed mathematical models predicting their pollutant emission behavior are extremely useful. These mathematical models must accurately describe the physical processes of fluid dynamics, heat and mass transfer, and also the chemical processes of combustion and pollutant formation. Clearly the predictions of a computer model can be only as good as these physical and chemical processes can themselves be modeled. Particularly important in predicting the pollutant emissions accompanying hydrocarbon combustion are the chemical mechanisms used to describe both the hydrocarbon combustion and pollutant formation. For the obvious practical reason of minimizing computation time, it is desirable to describe these chemical mechanisms in as few individual kinetic steps as possible. Hence, there is an apparent need to verify and optimize proposed chemical mechanisms.

The present experimental work was undertaken to provide a data base for such verification and optimization. The concentrations of total nitrogen oxides ( $\text{NO}_x$ ), carbon monoxide ( $\text{CO}$ ), and unburned hydrocarbons (UHC) generated by premixed methane-air flat flames were measured. These measurements were conducted at pressures from near atmospheric to 30 atm (1 atm = 101.3 kPa) because of the need to verify pollutant formation mechanisms over a range of pressures, typical of or encountered in practical combustion devices. The intent in using a flat flame for these measurements was to minimize, in future mathematical models of the flame, uncertainties in modeling the fluid dynamics and heat transfer in the flame. That is, if the physical aspects of the flame can be modeled with reasonable confidence, attention can be focused on the chemical mechanism in the model when making future comparisons of model predictions with experimental measurements.

During the course of this experimental investigation, several minor changes were made in the flameholder being used in the flat-flame burner. These minor changes produced unexpected changes in the pollutant emissions from the burner. The present paper describes the experimental investigation, the changes made in the flameholders, and the resulting pollutant emission data for  $\text{NO}_x$ ,  $\text{CO}$ , and UHC.

## EXPERIMENTAL PROCEDURE

### Flat-Flame Burner

The flat-flame burner was constructed of a thick-walled bronze burner body with a replaceable porous sintered bronze flameholder, 12.7 mm in diameter by 12.7 mm thick, mounted in the top center. (See fig. 1.) The cavity immediately upstream of the flameholder served as the mixing chamber. Fuel and air entered this cavity through radially opposed tubes to promote mixing. A quartz chimney, 20.5-mm inside diameter, was located concentric with the flameholder and extended 11 mm above its exit surface. The purpose of the chimney was to prevent the diffusion of combustion products into the surrounding gas, to prevent the surrounding gas from flowing into the flame zone, and to direct the combustion products from the flame upwards into an electrically heated sample collector located just above the quartz chimney. A ceramic collar, made of heat-treated hydrous aluminum silicate, surrounded the flameholder. This collar served as an insulator to minimize radial cooling of the flameholder, thereby promoting radial temperature uniformity of the flameholder and of the reactant gas mixture emerging from the flameholder. Removal of the heat absorbed from the flame by the flameholder was accomplished by means of a spring-loaded flat cooling coil in contact with the upstream side of the flameholder (not shown in fig. 1). Further details of the background work leading to the present burner design are given in reference 1.

### Pressure Chamber

The entire burner assembly was situated within a pressure chamber capable of pressurization to greater than 30 atm. (See fig. 2.) Nitrogen was used as

the pressurizing gas. Sight glass windows in the chamber permitted viewing the flame in a plane parallel with the flameholder surface. The total effluent from the chamber (combustion products and pressurizing nitrogen) flowed upward through the sample collector and transfer line and out through a back-pressure regulator, where the pressure was reduced to ambient. The sample collector and transfer line were heated electrically to prevent condensation of water vapor. The back-pressure regulator was enclosed within a housing which was swept with hot air (378 K) for the same purpose. After leaving the back-pressure regulator where the pressure was reduced to near atmospheric level, further heating of the combustion products was unnecessary to prevent condensation in the transfer lines to the analyzers, because the partial pressure of water vapor in the effluent was below the saturation vapor pressure of water at ambient conditions.

### Sample Analysis

From the back-pressure regulator, the effluent from the flame flowed to an analytical console where it was split for continuous analysis for  $\text{NO}_x$ , CO, UHC,  $\text{CO}_2$ , and  $\text{O}_2$ . The  $\text{NO}_x$  was determined by chemiluminescence, CO and  $\text{CO}_2$  by nondispersive infrared spectroscopy, UHC by flame ionization detection, and  $\text{O}_2$  by paramagnetism. Frequent recalibration of the instruments, with at least two calibration gases and a zero gas for each species, effectively eliminated errors due to instrument drift.

### Temperature Measurement

Flame temperatures were measured with a thermocouple probe. This probe was mounted in a pressure gland in the top of the pressure chamber above the burner and along its axis. (See fig. 2.) The thermocouple could be moved into the flame zone and retracted while the flame was burning. The thermocouple was Type B (Pt-6% Rh vs. Pt-30% Rh) with a 0.05-mm-diam butt-welded junction supported in a stirrup-type mount. It was not coated to prevent catalytic heating (as is sometimes done) because of the difficulties in applying such coatings and because of the unsatisfactory performance of such coatings reported by some investigators. For example, it was shown in reference 2 that thin coatings of silica on fine thermocouple wire, applied by the standard flame-spraying method of reference 3, can be destroyed even in fairly cool flames. Further, it was reported in reference 4 that similar coatings on coarse thermocouple wire can deteriorate in methane-air flames at temperatures as low as 1600 K, resulting in an alteration of the effective wire emissivity. A closed-circuit-television viewing system permitted observation of an enlarged view of the thermocouple in the flame. Details of the corrections required to account for catalytic heating of the thermocouple, and for radiation heat loss are described in appendix A.

Temperatures of the flameholder surface were determined using three 0.025-mm-diam Type K (Chromel-Alumel) thermocouples situated at three locations on the flameholder surface: at the center, midway between center and edge, and at the edge. Two of these thermocouples were laid in grooves, 0.25 mm wide

by 0.12 mm deep, cut into the flameholder surface by an electric discharge process, and a third was located at the edge of the flameholder. In order to make good thermal contact with the surface, the ball-type junction of each of these thermocouples was pressed into a small hole in the surface. The surface temperature of the flameholder was taken as the arithmetic average of the readings from these three thermocouples. Because of the low temperatures involved, no corrections were required to these thermocouple readings for radiation or catalytic heating.

#### Flameholders

Four porous sintered bronze flameholders were used in this study. Flameholder 1 had a maximum pore size of 25  $\mu\text{m}$  and was used without special surface treatment. Flameholder 2 was simply flameholder 1 after its surface has been polished with No. 600-grit emery paper and cleaned with an air blast applied to the opposite surface. Microscopic examination of its surface after this treatment revealed no particulate material stuck in the pores. Flameholder 3 was cut from a different grade of porous bronze stock and had a maximum pore size of 10  $\mu\text{m}$ . Flameholder 4 was flameholder 2 mounted in the inverted position (i.e., flameholder 4 was flameholder 2 with the inlet and outlet surfaces reversed). Thermocouple grooves were not cut in the exit surface of this last flameholder. A summary of these flameholders is given in the following table:

No.	Maximum pore size, $\mu\text{m}$	Thermocouple grooves on surface	Comments
1	25	Yes	No surface treatment
2	25	Yes	Flameholder 1 with polished surface
3	10	Yes	No surface treatment
4	25	No	Flameholder 2 inverted

Since the major goal of this investigation was to measure pollutant emissions over a range of combustion pressures from a well-defined combustion device, particular attention was paid to the uniformity and reproducibility of the burner flameholders and to the reproducibility of the experimental data. The surface of each flameholder was examined under the microscope for uniformity and imperfections. Flameholder 1 had been scanned for temperature uniformity across its surface in a bench test as described in reference 1. Results showed that the maximum temperature in the flame zone was uniform for about 2/3 of the radial distance from the center of the flameholder and decreased by only 9 percent of that value at 1 mm from the edge. Flameholders 2 and 4 were slightly modified versions of flameholder 1, as described. To reduce the possibility of systematic bias in the acquisition of the data, experimental runs were often made at different pressure levels from one run to

the next. Also, the experimental data for any one flameholder were taken typically over several month's time, rather than all being taken in one brief, uninterrupted sequence.

### Operation

To operate the flat-flame burner, the chamber was first pressurized with nitrogen to the desired pressure. Next, the methane ( $\text{CH}_4$ ) and air flow rates were set approximately to their desired values as indicated by individual mass flowmeters. The  $\text{CH}_4$  and  $\text{O}_2$  concentrations in the resulting combustible mixture were determined as the mixture flowed through the analytical console, and the flow rates were adjusted as necessary to obtain the desired mass flow rate and equivalence ratio conditions. The combustible mixture was then ignited by means of a small resistance-heated wire located near the lip of the chimney surrounding the burner. The flame flashed to a position just above the surface of the flameholder, where it stabilized. At higher pressure, particularly at 30 atm, the flames were more difficult to ignite and took longer to stabilize. This is probably because these flames are established closer to the burner surface, resulting in increased heat transfer to the burner. Pollutant concentrations in the effluent were continuously monitored on the analytical console until they reached a steady state. Maximum flame temperatures were measured by lowering the thermocouple probe towards the burner surface, passing slowly through the zone of maximum temperature in the flame, and slowly raising the thermocouple, withdrawing it from the flame. This technique gives two measurements for the maximum, or peak, temperature in the flame. After full retraction of the thermocouple, the flame was extinguished by a brief interruption of the fuel flow, and a second determination of the  $\text{CH}_4$  and  $\text{O}_2$  concentrations in the reactant mixture was made. Typically, differences between the before and after composition measurements were less than 1 percent. Equivalence ratios of the reactant mixtures were calculated using these composition measurements. The equivalence ratio for the run was taken to be a weighted time average of the before and after equivalence ratios. Experimental runs were made over the pressure range from 1.9 to 30 atm, for equivalence ratios from 0.84 to 1.12. Total reactant mass flow rates were held constant at about  $2740 \text{ cm}^3/\text{min}$  at STP, or about  $3.1 \text{ g/min}$ .

### RESULTS AND DISCUSSION

Data from the present study include data on maximum flame temperature and emissions concentrations for  $\text{NO}_x$ , CO, and UHC for the four flameholders. These data are presented in figures 3 to 6, respectively, as a function of pressure  $p$ , and equivalence ratio  $\phi$ . While there are obvious general similarities among these data for the four flameholders, certain differences in finer detail are also evident. These differences, which were not expected, are discussed in detail in the following sections.

## Visual Observations

Careful observation of the flames in this study revealed that some of them contained certain irregularities or disturbances. These irregularities and disturbances consisted of tilted flames, raised areas in the flame, flames with an occasional jumping (in space), flames with occasional flickering, or flames with a more regular fluctuation. Although these phenomena tended to be small, if they were observed at all, the flame in which they appeared was classified as unstable. Data from such flames are indicated by the solid symbols in figures 3 to 6. Flame instability was most prevalent for flameholders 2 and 3 and least for flameholder 1. Since these three flameholders all had thermocouple grooves in their surfaces, it is unlikely that the observed instabilities are caused by these grooves - especially in view of the fact that flameholder 4 had no such grooves, but still exhibited some instabilities. Because of the thinness of the reaction zones (as shown in ref. 1, reaction zones in flat flames may be as thin as 0.5 mm, or even less, at the higher pressures), there is a legitimate concern that the observed instabilities might affect the temperature and emissions measurements. However, such an effect does not appear to have occurred in view of the fact that, in figures 3 to 6, the data labeled "unstable" are fully consistent with the other data.

## Flame Temperature

The flame temperature data are shown in figure 3. These data represent the maximum temperature in the flame, obtained as described previously in the experimental section. For all flameholders, these flame temperature curves pass through a maximum near stoichiometric conditions, which is as expected. Also, there is a general trend towards decreasing flame temperature with increasing pressure for a constant equivalence ratio  $\phi$ . However, a closer look at the data reveals that the nature of this dependence of temperature on pressure differs somewhat for the different flameholders. For example, the temperatures for flameholders 1 and 4 are generally higher than those for flameholders 2 and 3. Also somewhat different are the locations of the maxima with respect to  $\phi$ . For flameholders 1 and 4, the locations of their maxima differ somewhat although there is rough agreement in the magnitudes of the temperatures (except for the 9.4-atm data); the temperatures for flameholder 1 peak near  $\phi = 0.99$ , while those for flameholder 4 tend to peak somewhat lower, near  $\phi = 0.95$  at the lower pressures. Note that both of these values are much lower than that for the peak in the curve of adiabatic flame temperature  $T_{ad}$  (calculated for a pressure of 2 atm), which occurs at about  $\phi = 1.03$ .

The magnitudes and shapes of the temperature curves in figure 3 are determined by a variety of factors. Although the maxima themselves arise solely from thermodynamics, why they are displaced towards lower values of  $\phi$  from that predicted by adiabatic equilibrium is not entirely clear. Some of this displacement could be caused by the method used to correct the raw thermocouple data for catalytic heating. This is because the method used (see app. A) is independent of  $\phi$ ; whereas, it is reasonable to expect that there really should be some dependence on  $\phi$ . Thus, the corrected flame temperatures possibly



could be prejudiced so as to produce the observed displacement. However, the displacement is also consistent with there being a somewhat higher heat loss to the burner for rich flames than for lean flames. That this might be the situation is indicated in figure 7, where the flameholder surface temperature, for the most part, is higher for rich flames than for lean flames. This would be the situation if, for instance, rich flames are established closer to the burner surface than are lean flames. Limited data in reference 1 suggest that flame zone thickness may vary with  $\phi$ , and, by extension, it seems reasonable that flame height may also.

The observed decrease in flame temperature in figure 3 with increasing pressure (at a given  $\phi$ ) is caused by increased heat loss to the burner as the flame height (the distance from the flameholder surface to the bottom of the flame zone) decreases. (Flame height decreases with increasing pressure because, at constant mass flow rate, the reactant velocity decreases.) That there is an increase in heat loss to the burner is evident from figure 7, where flameholder surface temperatures are seen to increase with increasing pressure. Several other factors also affect flame temperature, although these are second order in importance to those already mentioned. These factors include residence time, reaction rate, and radical species concentration - all of which vary with pressure. They are discussed in the following section in connection with factors affecting  $\text{NO}_x$  emissions.

#### $\text{NO}_x$ Emissions

Data on  $\text{NO}_x$  emissions are shown in figure 4 in terms of the molar emission index  $I_{\text{NO}_x}$ , defined as the moles of  $\text{NO}_x$  produced per mole of methane consumed. Experimentally,  $I_{\text{NO}_x}$  was determined by dividing the measured concentration of  $\text{NO}_x$  in the effluent from the chamber by the sum of the concentrations of CO and  $\text{CO}_2$ . The molar emission index, like temperature, shows both general similarities as well as certain differences among the four flameholders. The general characteristics of these data can be explained largely in terms of the temperature data already discussed. For instance, the curves of  $\text{NO}_x$  emissions as a function of equivalence ratio, with but two exceptions, pass through maxima near stoichiometric conditions and also show an overall trend to decrease with increasing pressure (at constant  $\phi$ ). As expected, the higher values of  $I_{\text{NO}_x}$  for flameholders 1 and 4 (relative to those of flameholders 2 and 3) are associated with higher temperatures for these flameholders. Yet, there are certain features of these  $I_{\text{NO}_x}$  data which cannot be explained in terms of the temperature data. For instance,  $I_{\text{NO}_x}$  for flameholder 1 peaks much more sharply than does  $I_{\text{NO}_x}$  for flameholder 4; whereas, the corresponding temperature data do not show such differences. Also, the change in  $I_{\text{NO}_x}$  with pressure, for a given value of  $\phi$ , is less for flameholder 1 than for flameholder 4. Again, the corresponding temperature data do not support these differences. And, for flameholder 1, the curves of  $I_{\text{NO}_x}$  at pressures below 20 atm are unique in that they tend to merge at the higher equivalence ratios. For flameholder 4, the 20-atm curve has an inverted shape and the 30-atm curve is peculiarly situated between the 10- and 20-atm curves. It is noted, however, that all data at 30 atm are from flames designated unstable. (See fig. 4(c).) Since it was not possible to obtain a 30-atm flame without some instability, it is not

possible to say whether this instability is responsible for the anomalous location of these data. The inverted shape of the 20-atm curve for flameholder 4, atypical as it is, was verified by a number of individual experimental runs expressly made for that purpose and is believed to be real. A similarly inverted 20-atm curve was also observed for flameholder 3, but not for flameholder 1. These inverted curves obviously are not caused by unusual temperature distributions at 20 atm, because the latter are perfectly regular. (See figs. 3(b) and 3(c).)

Another difference in the  $I_{NO_x}$  data observable among the four flameholders is the position of the maxima with respect to  $\phi$ . For flameholder 1, the maxima tend to larger values of  $\phi$  as the pressure is increased, while the opposite seems to be true for flameholders 2 and 3. For flameholder 4, there is little change in the position of the maxima except perhaps at the highest pressures, where the data become uncertain anyway. When the  $I_{NO_x}$  data are compared with the corresponding temperature data for each flameholder, the temperature peaks are seen to occur generally at about the same, or somewhat higher, values of  $\phi$  than the  $I_{NO_x}$  peaks. However, the indicated positions of these peaks in figures 3 and 4 are probably no better than  $\Delta\phi = \pm 0.02$ , because of scatter in the data. Hence, a strong emphasis cannot be placed on the precise value of these positions.

Besides temperature (which, as mentioned previously, varies inversely with pressure), pressure, by itself, has an influence on  $I_{NO_x}$ . For instance, an increase in pressure tends to increase  $I_{NO_x}$  by increasing both the reaction rate and the residence time of the reactants in the flame zone. But at the same time, it also acts to decrease  $I_{NO_x}$  by tending to lower the mole fraction of the radical species in the flame. The combined effect on  $I_{NO_x}$  from these several causes is considerably less than the effect that pressure has on  $I_{NO_x}$  by way of its effect on flame temperature. Because of these competing effects, the effective overall dependence of  $I_{NO_x}$  on pressure tends to be somewhat complicated. This dependence is treated in detail in appendix B, wherein a general equation relating  $I_{NO_x}$  to temperature, pressure, and  $\phi$  is developed. See, in particular, equation (B11). All the effects of pressure just discussed are, of course, in addition to any effect that pressure may have on  $I_{NO_x}$  by altering the chemical mechanism itself.

#### CO Emissions

The emissions data for CO are shown in figure 5 in terms of the molar emission index  $I_{CO}$ , defined as the moles of CO produced per mole of methane consumed. Experimentally,  $I_{CO}$  was determined from the effluent concentrations by dividing the measured concentration of CO by the sum of the concentrations of CO and  $CO_2$ . In general,  $I_{CO}$  for all four flameholders, notwithstanding the anomalous data for flameholder 1 (see fig. 5), is lowest at the low equivalence ratios and increases with increasing equivalence ratio. At constant  $\phi$ ,  $I_{CO}$  increases with pressure. This effect of pressure is more pronounced at the lower equivalence ratios; at the higher equivalence ratios,  $I_{CO}$  tends to approach a common value of about 0.25 for all pressures. As for  $I_{NO_x}$ , the effective overall dependence of  $I_{CO}$  on pressure involves separate

contributions of the effects of pressure on reaction rate, residence time, and mole fraction of flame radicals, in addition to the effect that pressure has on  $I_{CO}$  by way of its effect on flame temperature.

The overall character of the  $I_{CO}$  data is consistent with more oxygen being available for the conversion of CO to  $CO_2$  at the lower equivalence ratios. It is also consistent with the already observed fact that higher flame temperatures are reached by the lower pressure flames, causing a higher rate of conversion of CO to  $CO_2$  at these pressures. The approach of  $I_{CO}$  to a common value near 0.25 at the higher equivalence ratios is consistent with predictions from independent equilibrium calculations showing that  $I_{CO}$  approaches values of about 0.22 at  $\phi = 1.1$  and becomes largely independent of temperature and pressure. On the other hand, equilibrium values of  $I_{CO}$  at the lower equivalence ratios (at appropriate experimental values of temperature and pressure) bear little relationship to the present data. For example, these equilibrium values decrease extremely rapidly with increasing pressure - just the opposite of that experimentally observed - and tend to be considerably lower than the present data, particularly at the higher pressures. Clearly, kinetics is controlling the rate of production and destruction of CO at the lower equivalence ratios, but equilibrium CO concentrations are very likely approached at the higher equivalence ratios.

Comparison of the data for the several flameholders shows that, at constant pressure, the data for flameholders 2 and 3 have similar trends but are somewhat above those for flameholder 4. This, in turn, is consistent with the flame temperatures for flameholders 2 and 3 being somewhat lower than those for flameholder 4. Particularly curious are the data for flameholder 1. While these data show an overall increase in  $I_{CO}$  with increasing equivalence ratios similar to that for the other flameholders, the nature of the dependence of  $I_{CO}$  on  $\phi$  is strange indeed. These data are relatively insensitive to  $\phi$  at the very low values of  $\phi$ , but increase very rapidly as stoichiometric conditions are approached. Also, the curves of  $I_{CO}$  at constant pressure tend to cross one another - a phenomenon not observed for the remaining three flameholders. However,  $I_{CO}$  approaches a common value near 0.25 at the higher equivalence ratios, a behavior consistent with that of the other flameholders. No explanation is offered for the anomalous behavior of this flameholder.

#### Unburned Hydrocarbons

The emissions data for unburned hydrocarbons (UHC) are plotted in figure 6. As with the emissions data for  $NO_x$  and CO, these data are reported in terms of the molar emission index  $I_{UHC}$ , the moles of unburned hydrocarbons emitted per mole of methane consumed. It was calculated in a manner analogous to that for  $I_{NO_x}$  and  $I_{CO}$ . At constant pressure, the curves of  $I_{UHC}$  typically pass through minima slightly to the lean side of stoichiometric conditions. These curves tend to be broad and flat, with only moderate increases in  $I_{UHC}$  towards leaner and richer conditions. In view of the facts that these curves tend to be symmetric about their minima and that the corresponding flame temperature data are similarly symmetric, it would appear that flame temperature, and not  $\phi$ , is of greater importance in determining their shape. That is,

had  $\phi$  been the more important variable,  $I_{UHC}$  would be expected to be large at large  $\phi$  and small at small  $\phi$ . However, this is not the situation. Values of  $I_{UHC}$  calculated for equilibrium at all conditions of pressure, temperature, and  $\phi$ , are less than  $10^{-9}$ . Since the experimental values are six to eight orders of magnitude greater than these equilibrium values, the obvious implication is that equilibrium has not been even remotely approached and that substantial quantities of hydrocarbons are escaping from the flame uncombusted.

The index  $I_{UHC}$  increases with increasing pressure, as does  $I_{CO}$ . Whereas this increase in  $I_{UHC}$  is quite regular for flameholder 1, it is not so for flameholders 2 to 4. Comparisons of the magnitudes of the data at constant pressure for the several flameholders reveals certain significant differences. For instance, whereas the magnitude of  $I_{UHC}$  at 20 atm for flameholder 3 is similar to that for flameholder 1,  $I_{UHC}$  at the 9-atm level for flameholder 3 falls well below that for flameholder 1, while the data at 2 atm for flameholder 3 is only somewhat below that for flameholder 1. Likewise, the magnitudes of the curves of  $I_{UHC}$  at constant pressure are dissimilar between flameholders 1 and 4 - this, in spite of the fact that the flame temperatures for these two flameholders are in reasonable agreement. The  $I_{UHC}$  curves for flameholder 4 at the lower pressures are anomalously close together, while the spacing between the curves at the higher pressures seems more regular. This behavior is not related to a similarly unusual behavior of the temperature data, and its explanation is not known.

## Discussion

All emissions data have been presented in terms of an emission index based on the moles of methane consumed. This basis was used because the  $NO_x$  and CO emissions occur solely as a direct result of the methane being combusted. However, an alternate emission index - one based on the moles of methane fed to the burner - could also have been used. There would be little difference between the values of these two indices at the lower pressures where the amount of unburned hydrocarbons is small. (See fig. 6.) But, at the higher pressures where the amount of unburned hydrocarbons becomes appreciable, the values of the two indices would be somewhat different. Specifically, if the alternate definition (i.e., the one based on the moles of methane fed to the burner) had been used in figures 4 to 6, the curves would be displaced downward by the factor  $1/(1 + I_{UHC})$ . A consideration of figure 6 for  $I_{UHC}$  shows that such displacement becomes significant only at the higher pressures of 20 or 30 atm. But the basic shapes of the curves would largely be retained because, at constant pressure, the change in  $I_{UHC}$  with  $\phi$  is relatively small. Furthermore, the relative positions of the curves would be unchanged. Although for the present purposes there seems to be little to be gained by using this alternate definition, for other purposes it could be preferable.

Careful examination of the temperature and emissions data for all four flameholders fails to identify any one flameholder as producing data most representative of what would be expected for an idealized flat flame. Since each flameholder has associated with it at least one set of anomalous data,

there is no basis on which any one can be singled out. For example, flame temperatures for flameholders 2 and 3 seem low relative to those of the other two, and  $I_{NO_x}$  for flameholders 3 and 4 shows unexplained peculiarities at the higher pressures. These differences, and others for  $I_{CO}$  and  $I_{UHC}$ , are believed to be caused by minor variations in the surfaces of the flameholders themselves. This conclusion seems inescapable in view of the fact that the bodies of flameholders 1, 2, and 4 were identical - only their exit surfaces were slightly different.

The implication of the observed diverse behavior of the various flameholders is that close attention needs to be given the burner flameholder to insure that representative data are obtained. Certainly, it would be prudent to use more than one flameholder to obtain the desired data. Without such precautions, it would seem easily possible to accept as representative some data which, in fact, contain minor distortions caused by burner-induced effects. For the present data, attention should be focused primarily on the more general features of the temperature and emissions data in seeking to verify a kinetic mechanism describing combustion and/or pollutant formation. Attention to the finer details could lead to unwarranted conclusions because these are likely artifacts of the particular burners.

#### Correlations of $NO_x$ Data

Although the finer details of the  $NO_x$  emissions data differ among the various flameholders, the overall characteristics are sufficiently regular and the dependence on maximum flame temperature is sufficiently strong to justify correlating  $I_{NO_x}$  in terms of temperature. It is also of considerable practical interest to determine, if possible, whether and how  $I_{NO_x}$  depends on pressure  $p$  and on  $\phi$ .

A general expression for correlating  $I_{NO_x}$  which accounts for both flame-produced, or thermal, NO and prompt NO (ref. 5), can be written

$$I_{NO_x} = \left( \frac{1 + 0.105\phi}{0.105\phi} \right) \left[ A \frac{1}{T^2} e^{-\theta/T} p^{2-s-n(\phi)} + B(\phi - 0.8) e^{-20000/T} p^{1/2} \right] \quad (1)$$

where  $T$  is the maximum flame temperature,  $A$ ,  $\theta$ ,  $B$ , and  $s$  are constants, and  $n(\phi)$  is an undetermined function of  $\phi$ . The details of the development of this expression are given in appendix B. Taking  $n(\phi) = -m\phi + (2 - s)$ , where  $m$  is a constant, a correlation of the combined data for all four flameholders was sought in this form by a minimization of squares technique. Values obtained for the constants (for  $p$  in atm,  $T$  in K) were  $A = 2100$ ,  $\theta = 5230$  K,  $m = -0.26$ , and  $B = 0.27$ , with an average residual for the correlation of about 13 percent. Based on this correlation, the contribution of prompt NO (the second term in eq. (1)) to the total NO, at  $\phi = 1$ , is on the order of 20 percent at typical flame conditions.

Strictly speaking, however, this correlation is not mathematically valid. This is because  $T$  is not really an independent variable but is, instead,

dependent on both  $p$  and  $\phi$ . That is,  $T$  is actually a dependent variable and properly should not be included with the truly independent variables  $p$  and  $\phi$  on the right-hand side of the equation. But since it is not mathematically possible to separate out  $T$  and since  $T$  contains the influence of  $p$  and  $\phi$  anyway, a convenient expression for correlating the data is  $I_{NO_x}$  written simply in terms of  $T$  only. On this basis, equation (1) reduces to

$$I_{NO_x} = A \frac{1}{T^2} e^{-\theta/T} \quad (2)$$

This expression, although mathematically more defensible than equation (1), contains less information because the dependencies of  $p$  and  $\phi$  are buried entirely in  $T$ . By a least squares minimization, it is found that  $A = 3.29 \times 10^5$  and  $\theta = 10\,960$  K with an average residual of about  $16\frac{1}{2}$  percent, not a great deal larger than that for the more complicated expression of equation (1).

The correlation given by equation (2), along with the  $I_{NO_x}$  data for all four flameholders, is shown in figure 8 plotted as a function of  $T^{-1}$ . Error bounds have been drawn about the correlation line representing  $\pm 50$  K and  $\pm 10$  percent  $I_{NO_x}$ . Roughly 75 percent of the data fall within these error bounds. Note that most of the scatter in the data occur at the lower temperatures, which also is the region of higher pressures. The scatter here is not surprising because flame temperatures become more difficult to measure accurately at the higher pressures (the reaction zone becomes very thin and rapid fluctuations appear in the raw thermocouple data) and  $NO_x$  concentrations become small. However, it is believed that not all the scatter in the data (at any temperature) can be ascribed to experimental error. Very likely there are real variations in  $I_{NO_x}$  caused by  $p$  and  $\phi$  which are not accounted for in this simplified correlation. Unfortunately, attempts to determine the true nature of these effects from the present data have been unsuccessful. This is partially because the scatter in the data may mask some of these effects, but also because real differences exist among the data from the four flameholders. Particularly helpful for defining the role of  $p$  and  $\phi$  would be  $I_{NO_x}$  data at constant  $p$  and  $\phi$  in which  $T$  is varied independently (i.e., by varying reactant mass flow rate). To explain the anomalous behavior of the  $I_{NO_x}$  data at the higher pressures (i.e., at pressures of 20 atm or above), the possibility that some additional mechanism or influence is coming into play should not be discounted. Such may be related to changes in flow patterns, heat loss to the burner, diffusion of radicals, or other factors. The possibility of such additional influences on the data deserves further investigation.

## CONCLUSIONS

Maximum flame temperatures and pollutant emissions for  $NO_x$ , CO, and UHC have been measured for methane-air flat flames at constant total mass flow rate over the pressure range from 1.9 to 30 atm and for equivalence ratios from 0.84 to 1.12. On the basis of these data, the following conclusions are offered:

1. At constant equivalence ratio, flame temperature and  $\text{NO}_x$  emissions decrease with increasing pressure, while CO and UHC emissions increase with increasing pressure. The changes in emissions are believed to be caused more by the decrease in temperature than by the increase in pressure.
2. The decrease in flame temperature with increasing pressure is due to increased heat transfer to the burner as the flame approaches the burner.
3. The data on  $\text{NO}_x$  emissions correlate reasonably well in terms of flame temperature only. Although these emissions are also believed to depend to some degree on pressure and equivalence ratio, the nature of these dependencies could not be established.
4. On the whole, the temperature and  $\text{NO}_x$  emissions, for any given pressure, typically attain maxima slightly to the lean side of stoichiometric conditions. The UHC emissions attain minima at roughly these same equivalence ratios. In contrast, the CO emissions generally increase continually with increasing equivalence ratio, showing no extrema.
5. Chemical equilibrium is not attained by the flames, as evidenced by the fact that experimental values of  $I_{\text{UHC}}$  are considerably greater than theoretical equilibrium values.
6. In measurements on flat-flame burners, flameholders which differ only slightly in the condition of their surfaces can give somewhat different temperature and emissions data.
7. For the present temperature and emissions data, attention should be focused primarily on the more general features; close attention to the finer details of these data could lead to unwarranted conclusions because these are likely to be artifacts of the particular burners.
8. To ensure that flat-flame data are free from burner-induced effects, it would appear prudent to verify such data by using more than one flameholder or burner.

Langley Research Center  
National Aeronautics and Space Administration  
Hampton, VA 23665  
May 1, 1980

## APPENDIX A

### THERMOCOUPLE CORRECTIONS

The equation for the conservation of energy applicable to a thermocouple in a flame can be written (ref. 2):

$$Q_{\text{cat}} + Q_{\text{conv}} = Q_{\text{rad}} + Q_{\text{cond}} \quad (\text{A1})$$

where  $Q$  is the net rate of energy transport per unit area of the thermocouple wire and the subscripts refer, respectively, to catalytic heating of the wire (by radical recombination on the surface), convection to the wire, radiation from the wire, and conduction along the wire away from the thermocouple junction. Expressions for these transport rates are given by (ref. 2):

$$Q_{\text{cat}} = \sum_i Z_i [i]_s \gamma_i \alpha_i \Delta H_i$$

$$Q_{\text{conv}} = h(T_f - T_c)$$

$$Q_{\text{rad}} = \sigma \epsilon (T_c^4 - T_w^4)$$

$$Q_{\text{cond}} \approx 0$$

where

$Z_i$  collision frequency of radical  $i$  per unit concentration per unit area of the surface

$[i]_s$  concentration of radical  $i$  at the surface

$\gamma_i$  surface recombination coefficient

$\alpha_i$  thermal accommodation coefficient

$\Delta H_i$  heat of recombination

$h$  convective heat transfer coefficient

$T_f$  flame temperature

$T_c$  thermocouple junction temperature

$\sigma$  Stefan-Boltzmann constant

$\epsilon$  thermocouple emissivity

$T_w$  temperature of the surroundings



# APPENDIX A

After substituting the above expressions for  $Q$  into equation (A1), taking  $T_w^4 \ll T_c^4$ , dividing by  $h$ , and rearranging, there results

$$T_f = T_c + \left( \frac{\sigma \epsilon}{h} T_c^4 \right) - \left( \sum_i \frac{Z_i \gamma_i [i]_s}{h} \alpha_i \Delta H_i \right) \quad (A2)$$

This expression gives explicitly the corrections for radiation and catalytic heating which must be applied to the experimental thermocouple temperature to obtain the flame temperature.

The radiation correction term, the second term on the right-hand side of equation (A2), was determined by substituting for  $h$  the expression (ref. 3)

$$h = 0.8 \left( \frac{k}{d} \right) \left( \frac{d \rho v}{\mu} \right)^{1/4} \quad (A3)$$

where  $k$  is the thermal conductivity,  $\rho$  the density,  $v$  the velocity, and  $\mu$  the viscosity of the flame gases adjacent to the thermocouple, and  $d$  is the diameter of the thermocouple junction. Designating the radiation correction term as  $\Delta T_{rad}$ , we have

$$\Delta T_{rad} \equiv \frac{\sigma \epsilon}{h} T_c^4 = \frac{1.25 \sigma \epsilon d^{3/4} (\mu / \rho v)^{1/4}}{k} T_c^4$$

To evaluate this expression,  $\epsilon$  was taken to be 0.25 (refs. 6 to 8),  $k$  and  $\mu$  were evaluated at the thermocouple temperature (for a stoichiometric mixture of nitrogen, carbon dioxide, and water vapor), and  $\dot{m}_T/A$  was substituted for  $\rho v$ , where  $\dot{m}_T/A$  is the total mass flux through the burner.

The catalytic heating correction term, the last term on the right-hand side of equation (A2), also needs to be determined. In those situations when  $\gamma_i \rightarrow 0$  (such as on noncatalytic surfaces) or when  $Z_i [i]_s \rightarrow 0$  (as would be the situation at high pressures), no significant catalytic heating occurs and no corrections are necessary. But, since these conditions are not met for the conditions in the present study, a suitable correction must be made. Following reference 2, the expression for the conservation of species  $i$  can be written

$$Z_i \gamma_i [i]_s = h_D ([i] - [i]_s)$$

where  $h_D$  is the mass diffusion coefficient for species  $i$ , and  $[i]$  is the concentration of  $i$  in the bulk gas. This equation arises by setting the rate of recombination of  $i$  on the thermocouple surface equal to the rate of diffusion of  $i$  to the surface. By the assumption (ref. 2) of diffusion control (i.e., that  $[i]_s \ll [i]$ ), this expression reduces to

$$Z_i \gamma_i [i]_s = h_D [i] \quad (A4)$$

## APPENDIX A

By appealing to the analogy between heat and mass transfer and by making the unity Lewis number approximation, it can be shown that

$$h_D = \frac{h}{c_p \rho} \quad (A5)$$

where  $c_p$  is the specific heat of the flame gases. Designating the catalytic heating term as  $\Delta T_{cat}$  and using equations (A4) and (A5), there is obtained

$$\Delta T_{cat} \equiv \sum_i \frac{z_i \gamma_i [i]_s}{h} \alpha_i \Delta H_i = \sum_i \frac{[i]}{c_p \rho} \alpha_i \Delta H_i \quad (A6)$$

Using the perfect gas law for  $\rho$ , rewriting the concentrations  $[i]$  in terms of mole fractions  $x_i$ , and taking the  $\alpha_i$  to be unity (ref. 2) results in

$$\Delta T_{cat} = \sum_i \frac{x_i}{\hat{c}_p} \Delta H_i \quad (A7)$$

where  $\hat{c}_p$  is the molar heat capacity of the flame gases. Both  $\Delta H_i$  and  $\hat{c}_p$  are independent of pressure and only weak functions of temperature. Furthermore,  $\Delta H_i$  does not vary substantially with the nature of the radical species (e.g.,  $\Delta H_i$  differs by only about 11 percent for O-atoms and H-atoms). Hence, a reasonable approximation for equation (A7) is

$$\Delta T_{cat} \approx x_r \quad (A8)$$

where  $x_r$  is the total mole fraction of the radical species in the flame.

In order to use equation (A8), a way must first be found to relate  $x_r$  to the combustion pressure  $p$ . The approach used is as follows: When the thermocouple was inserted into the flame, the species concentrations being monitored were invariably perturbed. Typically, CO, O<sub>2</sub>, and UHC increased and NO<sub>x</sub> and CO<sub>2</sub> decreased. Since these perturbations are consistent with a mechanism of catalytic recombination of flame radicals on the thermocouple, they can be used as an indication of the relative radical concentration in the flame. That is, these perturbations, which are evidence of a change in the radical concentration in the flame, should be proportional to the radical concentration existing in the unperturbed flame. And, as such, they can be used as an indication of how the radical concentration varies with pressure. For an estimate of this variation, the NO<sub>x</sub> measurements are particularly useful because the perturbations for NO<sub>x</sub> are larger and can be more accurately measured, than those for the other species. Shown in figure 9 is a plot of the change in NO<sub>x</sub> concentration produced by the thermocouple  $\Delta NO_x$  as a function of pressure. These values have been normalized to the change in NO<sub>x</sub> at 1.9 atm for flameholder 1 and to the change in NO<sub>x</sub> at 2.0 atm for flameholder 4. Although it seems reasonable to expect that  $\Delta NO_x$  might vary somewhat with  $\phi$ , no clear dependence on  $\phi$  was observed when  $\Delta NO_x$  was plotted as a function of  $\phi$  at

## APPENDIX A

constant pressure for these two burners. Hence, figure 9 is the best representation of the data for all  $\phi$ . The slope of the line through these data is  $-3/2$ , implying that  $x_r$  varies roughly as  $p^{-3/2}$ . Thus, equation (A8) becomes

$$\Delta T_{\text{cat}} \approx p^{-3/2} \quad (\text{A9})$$

Although useful for the present purpose of correcting for catalytic heating, equation (A9), in spite of its appearance, is not a general expression giving  $\Delta T_{\text{cat}}$  as a function of  $p$  at constant  $T$ . This is because  $T$  itself is a function of  $p$ , and this dependence is inherent in the development of equation (A9). For the present purposes, however, it is neither necessary nor desirable to separate out the dependence on temperature. This only would have been necessary had it been desired to develop an expression for  $\Delta T_{\text{cat}}$  for a situation in which  $T$  and  $p$  were mutually independent. (In this situation, an expression for  $x_r$  in eq. (A8) would have to be developed to give the explicit dependence of  $x_r$  on both  $T$  and  $p$ .)

To evaluate the constant in equation (A9),  $\Delta T_{\text{cat}}$  at  $p = 2$  atm was taken to be 100 K - this being the proper order of magnitude needed to give a final corrected flame temperature somewhat below adiabatic flame temperature. Although this value of 100 K is admittedly somewhat arbitrary, based on the available raw data and the calculated adiabatic flame temperature, it is believed to be within  $\pm 50$  K of the true value and is likely within  $\pm 25$  K. Using this value for  $\Delta T_{\text{cat}}$ , the final expression for use in equation (A2) becomes

$$\Delta T_{\text{cat}} = 283 p^{-3/2} \quad (\text{A10})$$

## APPENDIX B

### EXPRESSIONS FOR CORRELATING NO<sub>x</sub> DATA

The concentration of NO<sub>x</sub> leaving a flame can be expressed as the sum of the contributions from thermal NO and from prompt NO,

$$C_{NO_x} = (C_{NO})_{\text{thermal}} + (C_{NO})_{\text{prompt}} \quad (B1)$$

If the thermal NO is from a Zeldovich-type mechanism (see, for instance, ref. 9),

$$\frac{d(C_{NO})_{\text{thermal}}}{dt} \propto e^{-\theta/T} C_{N_2} C_O$$

where  $\theta$  is the activation temperature and  $C_{N_2}$  and  $C_O$  are the nitrogen and atomic-oxygen concentrations, respectively. Integration of this rate expression at average constant temperature  $T$  and average concentrations  $C_i$  over a characteristic residence time  $\tau$  yields

$$(C_{NO})_{\text{thermal}} \propto e^{-\theta/T} C_{N_2} C_O \tau \quad (B2)$$

Residence time is defined by

$$\tau = \frac{t_f}{v_f} \quad (B3)$$

where  $t_f$  is the thickness of the flame and  $v_f$  is the flame velocity. This velocity can, in turn, be expressed as

$$v_f = \frac{\rho v}{\rho_f} \propto \frac{T}{p} \quad (B4)$$

where the perfect gas law has been used to express the average density in the flame  $\rho_f$  in terms of the temperature and pressure of the flame and where use has been made of the fact that the  $\rho v$  product is the total reactant mass flux (i.e.,  $\rho v = \dot{m}_T/A$ , a constant). Based on data from reference 1, the flame thickness at constant mass flow rate can be expressed as

$$t_f \propto p^{-n(\phi)} \quad (B5)$$

where the exponent  $n(\phi)$  is an (undetermined) function of  $\phi$  and where the negative sign in the exponent indicates that as  $p$  increases  $t_f$  decreases.

## APPENDIX B

Substitution of equations (B4) and (B5) into equation (B3) gives the residence time,

$$\tau \propto \frac{p^{1-n(\phi)}}{T} \quad (B6)$$

Further, substitution of this equation and equation (B2) into equation (B1) gives, after rewriting the concentrations  $C_i$  in terms of mole fractions  $x_i$ ,

$$x_{NO_x} \propto \frac{1}{T^2} e^{-\theta/T} p^{2-n(\phi)} x_{N_2} x_O + (x_{NO})_{prompt} \quad (B7)$$

An approximate expression for  $(x_{NO})_{prompt}$  for use in equation (B7) can be developed for methane combustion from data reported in reference 5. These data indicate an activation temperature of formation of about 20 000 K and a pressure dependence of about 1/2. Further,  $(x_{NO})_{prompt}$  approaches zero as  $\phi$  decreases towards 0.8. These facts may be conveniently expressed as

$$(x_{NO})_{prompt} = B(\phi - 0.8) e^{-20\,000/T} p^{1/2} \quad (B8)$$

where  $B$  is an undetermined constant. After substituting this expression into equation (B7) and dividing by the mole fraction of methane  $x_{CH_4}$ , there is obtained

$$\begin{aligned} I_{NO_x} \equiv \frac{x_{NO_x}}{x_{CH_4}} &\propto \frac{1}{x_{CH_4} T^2} e^{-\theta/T} p^{2-n(\phi)} x_{N_2} x_O \\ &+ \frac{B}{x_{CH_4}} (\phi - 0.8) e^{-20\,000/T} p^{1/2} \end{aligned} \quad (B9)$$

where use has been made of the definition

$$I_{NO_x} \equiv \frac{(n_{NO_x})_{produced}}{(n_{CH_4})_{consumed}} = \frac{(C_{NO_x})_{produced}}{(C_{CH_4})_{consumed}} = \frac{(x_{NO_x})_{produced}}{(x_{CH_4})_{consumed}} = \frac{x_{NO_x}}{x_{CH_4}}$$

where  $n_i$  refers to the number of moles of species  $i$ . (Note that  $I_{NO_x}$  can be written in terms of the concentrations as indicated above because there is negligible molar change in the methane combustion reaction.) From the definition of  $\phi$ ,

# APPENDIX B

$$\phi \equiv \frac{x_{CH_4}/x_{air}}{(x_{CH_4}/x_{air})_{stoich}}$$

and the fact that  $x_{CH_4} + x_{air} = 1.0$ ,  $x_{CH_4}$  in equation (B9) can be written in terms of  $\phi$  as

$$x_{CH_4} = \frac{0.105 \phi}{1 + 0.105 \phi} \quad (B10)$$

To a good approximation, the mole fraction  $x_{N_2}$  is a constant. Making these substitutions in equation (B9) and taking  $x_O$  to be in the form

$$x_O = g(\phi) e^{-\theta'/T} p^{-s}$$

where  $g(\phi)$  is a function of  $\phi$  (presumed weak),  $\theta'$  is an activation temperature (small), and  $s$  is a constant (expressing the decrease in  $x_O$  with increasing pressure), there results

$$I_{NO_x} = \left( \frac{1 + 0.105 \phi}{0.105 \phi} \right) \left[ A \frac{1}{T^2} e^{-\theta/T} p^{2-s-n(\phi)} + B(\phi - 0.8) e^{-20\,000/T} p^{1/2} \right] \quad (B11)$$

after having taken  $g(\phi)$  to be approximately constant and having combined  $\theta'$  (which is likely much smaller than  $\theta$ ) with  $\theta$  into a single new exponent  $\theta$ . In this equation,  $A$ ,  $\theta$ ,  $B$ , and  $s$  are constants and  $n(\phi)$  is an undetermined function of  $\phi$ . For the situation of all thermal NO being produced by a Zeldovich mechanism, the value of  $\theta$  should be about 38 000 K (see, for instance, ref. 9).

#### REFERENCES

1. Miller, Irvin M.: A High-Pressure Premixed Flat-Flame Burner for Chemical Process Studies. NASA TP-1318, 1978.
2. Hayhurst, A. N.; and Kittelson, D. B.: Heat and Mass Transfer Considerations in the Use of Electrically Heated Thermocouples of Iridium Versus an Iridium/Rhodium Alloy in Atmospheric Pressure Flames. Combust. & Flame, vol. 28, no. 3, 1977, pp. 301-317.
3. Kaskan, W. E.: The Dependence of Flame Temperature on Mass Burning Velocity. Sixth Symposium (International) on Combustion, Reinhold Pub. Corp., c.1957, pp. 134-143.
4. Miller, Irvin M.: The Measurement of Flame Temperatures With Coated, Electrically Heated Thermocouples. M. A. Thesis, The College of William and Mary in Virginia, 1971.
5. Fenimore, C. P.: Formation of Nitric Oxide in Premixed Hydrocarbon Flames. Thirteenth Symposium (International) on Combustion, Combustion Inst., 1971, pp. 373-380.
6. Glawe, George E.; and Shepard, Charles E.: Some Effects of Exposure to Exhaust-Gas Streams on Emittance and Thermoelectric Power of Bare-Wire Platinum Rhodium - Platinum Thermocouples. NACA TN 3253, 1954.
7. Sarofim, A. F.; and Pohl, J. H.: Kinetics of Nitric Oxide Formation in Premixed Laminar Flames. Fourteenth Symposium (International) on Combustion, Combustion Inst., 1973, pp. 739-754.
8. Takagi, Toshimi; Ogasawara, Mitsunobu; Fujii, Kenichi; and Daizo, Masahito: A Study on Nitric Oxide Formation in Turbulent Diffusion Flames. Fifteenth Symposium (International) on Combustion, Combustion Inst., 1974, pp. 1051-1059.
9. Miller, Irvin M.; and Maahs, Howard G.: High-Pressure Flame System for Pollution Studies With Results for Methane-Air Diffusion Flames. NASA TN D-8407, 1977.

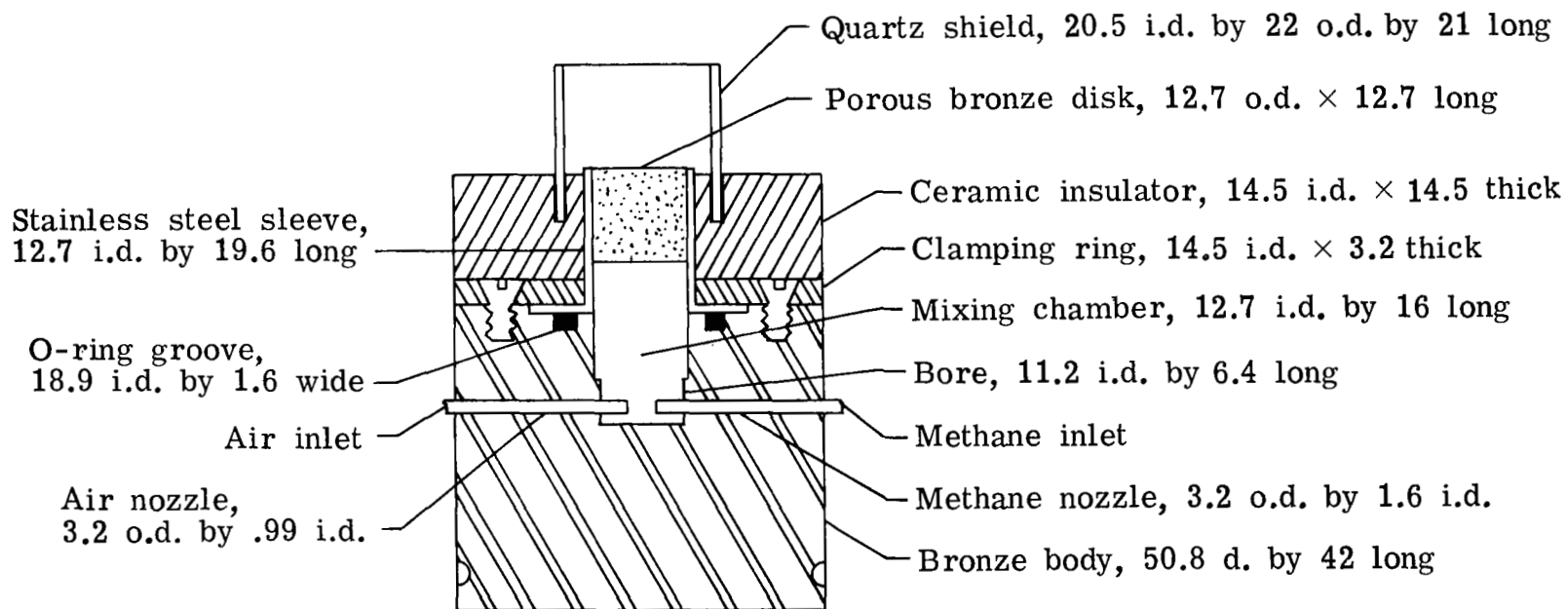


Figure 1.- Flat-flame burner. All dimensions in mm.



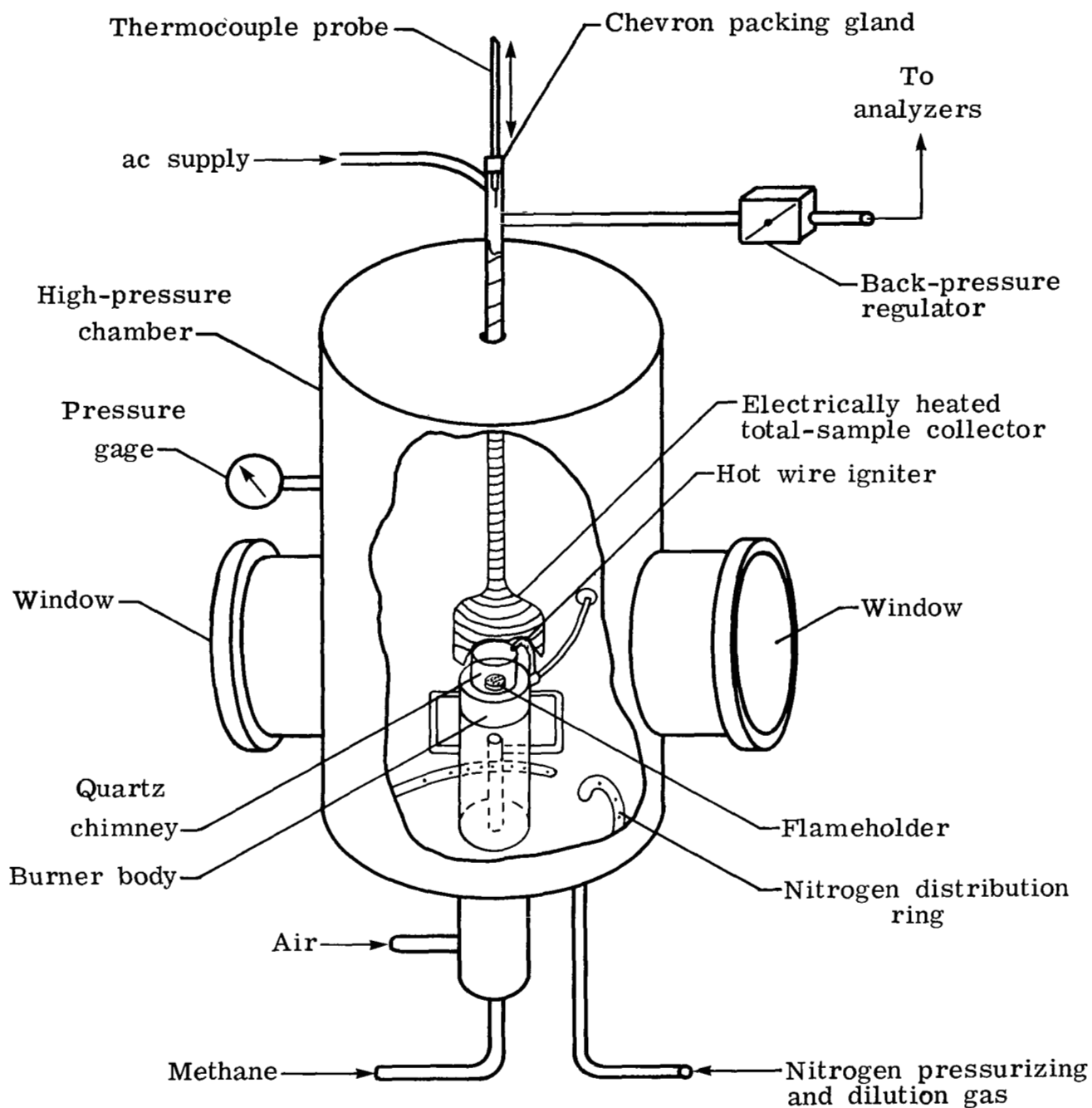
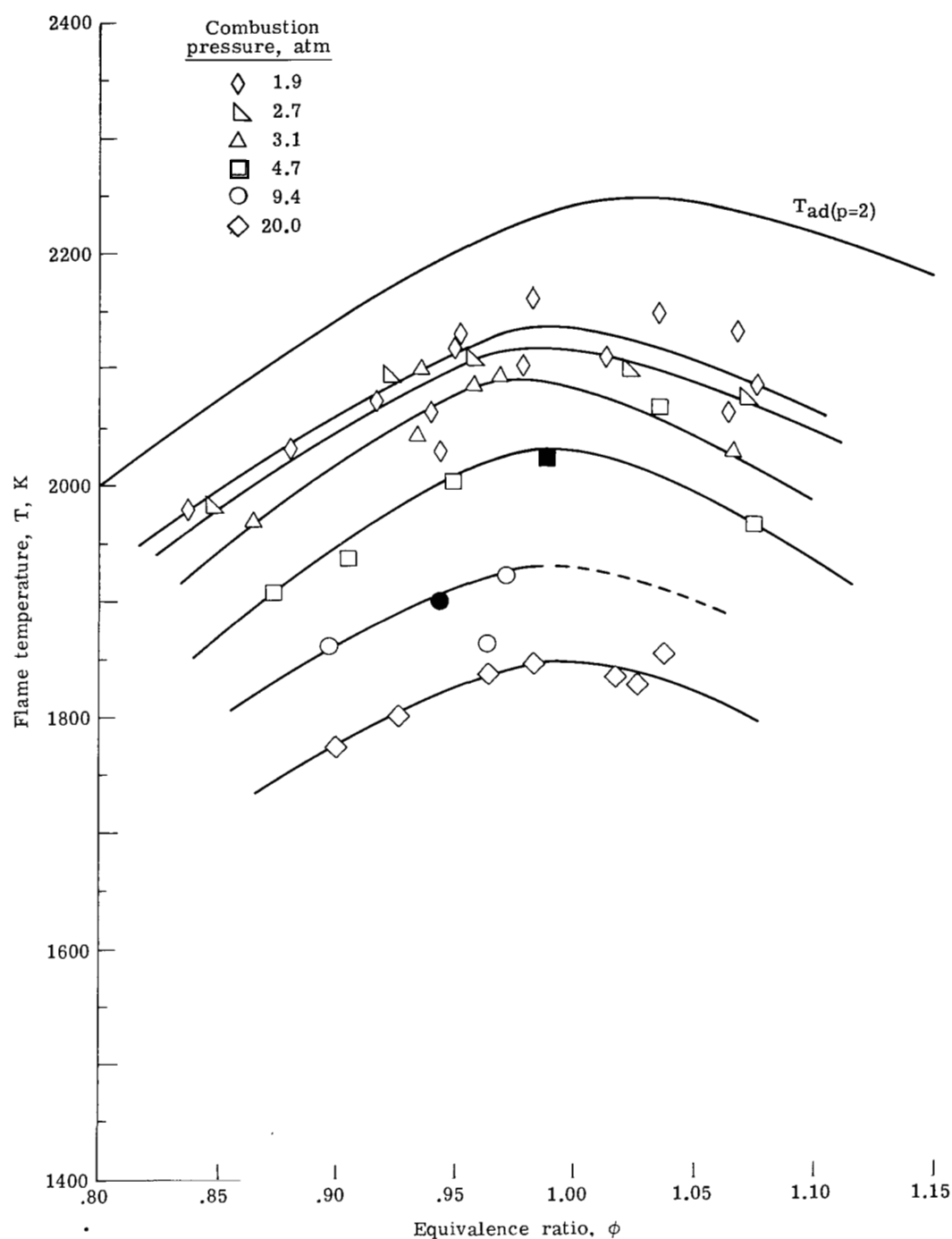
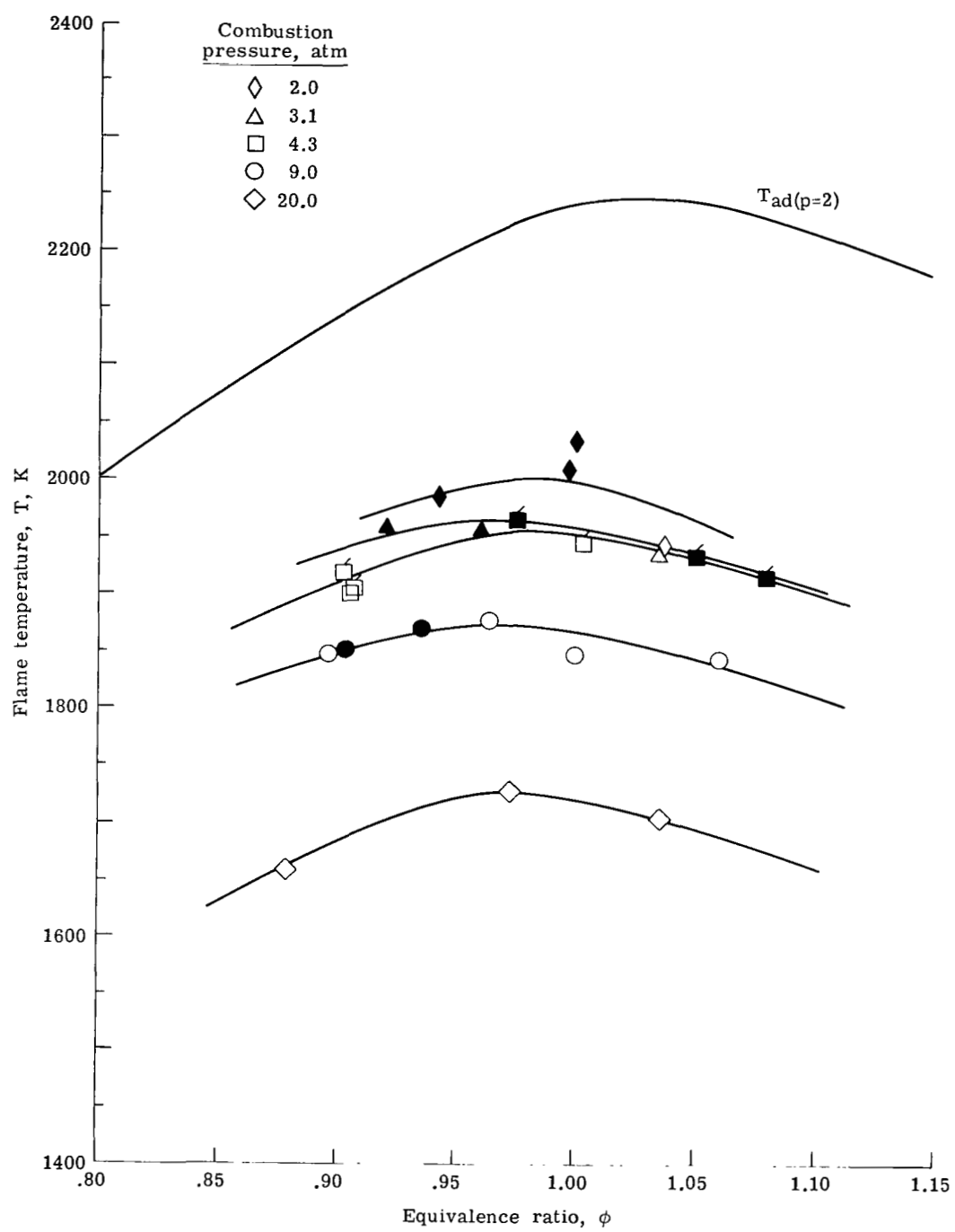


Figure 2.- Schematic diagram of high-pressure chamber, burner, and sample collection system.



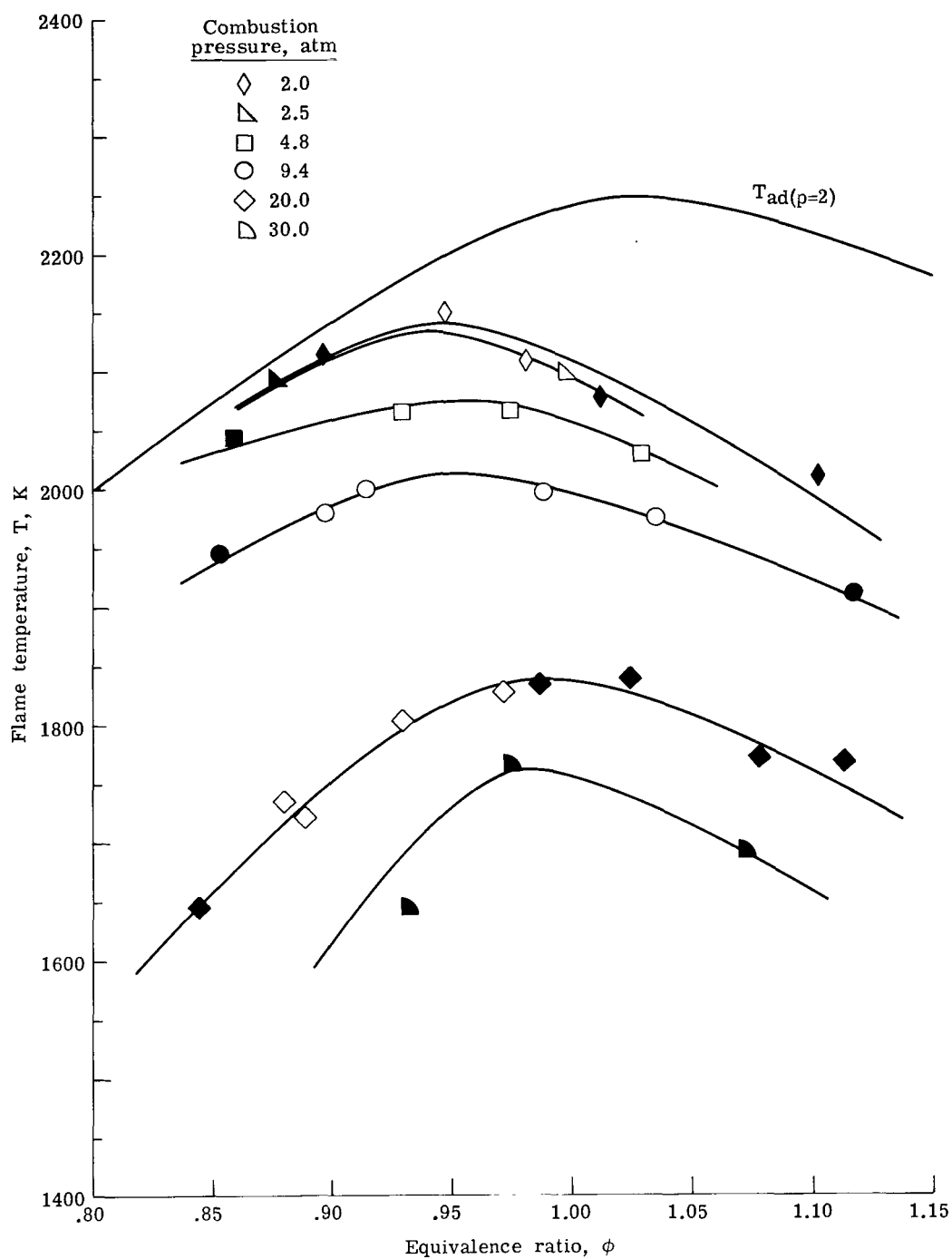
(a) Flameholder 1.

Figure 3.- Maximum flame temperature as function of pressure and equivalence ratio.  $T_{ad}(p=2)$  is adiabatic flame temperature at 2 atm. Solid symbols: unstable flame.



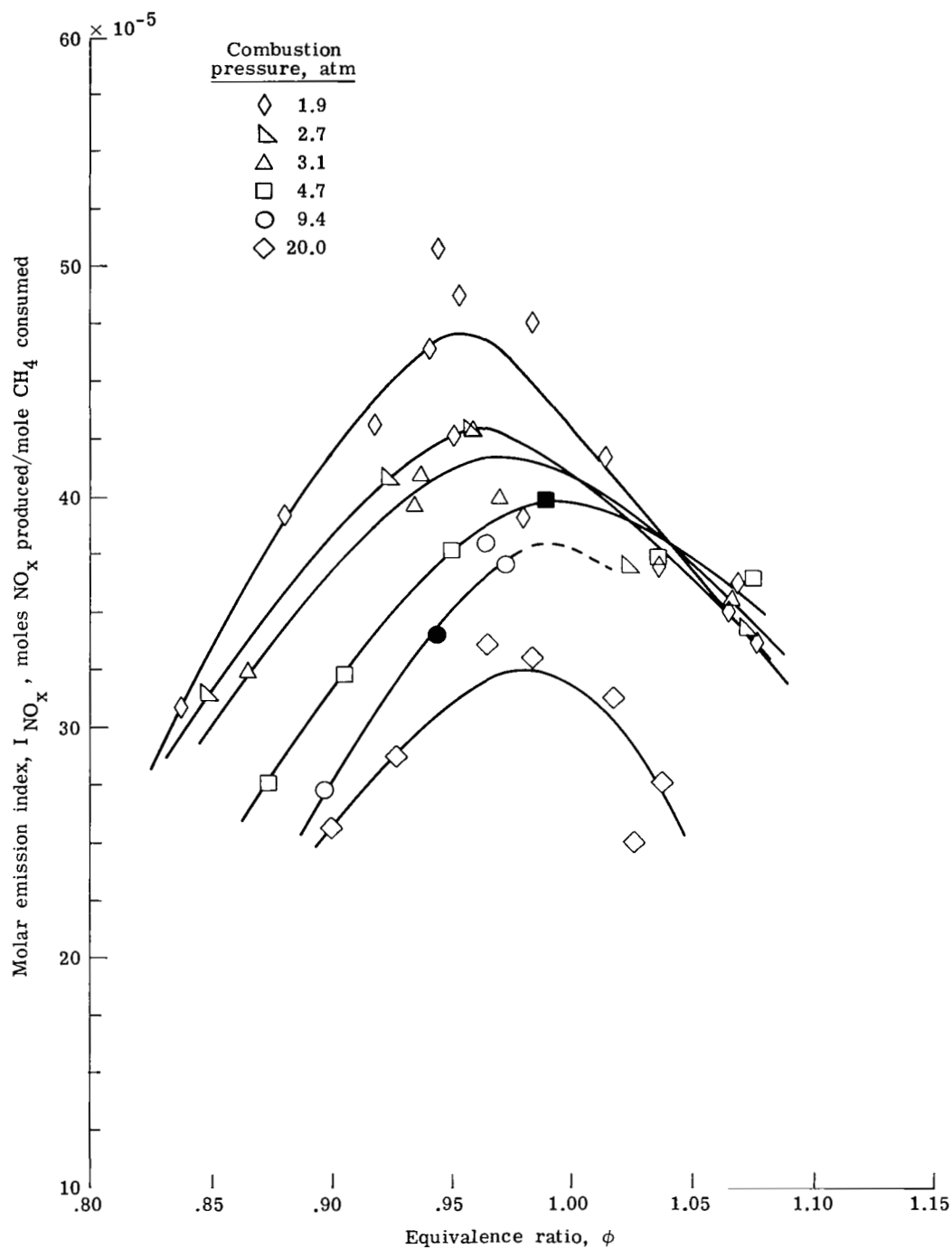
(b) Flameholders 2 (marked with flag) and 3.

Figure 3.- Continued.



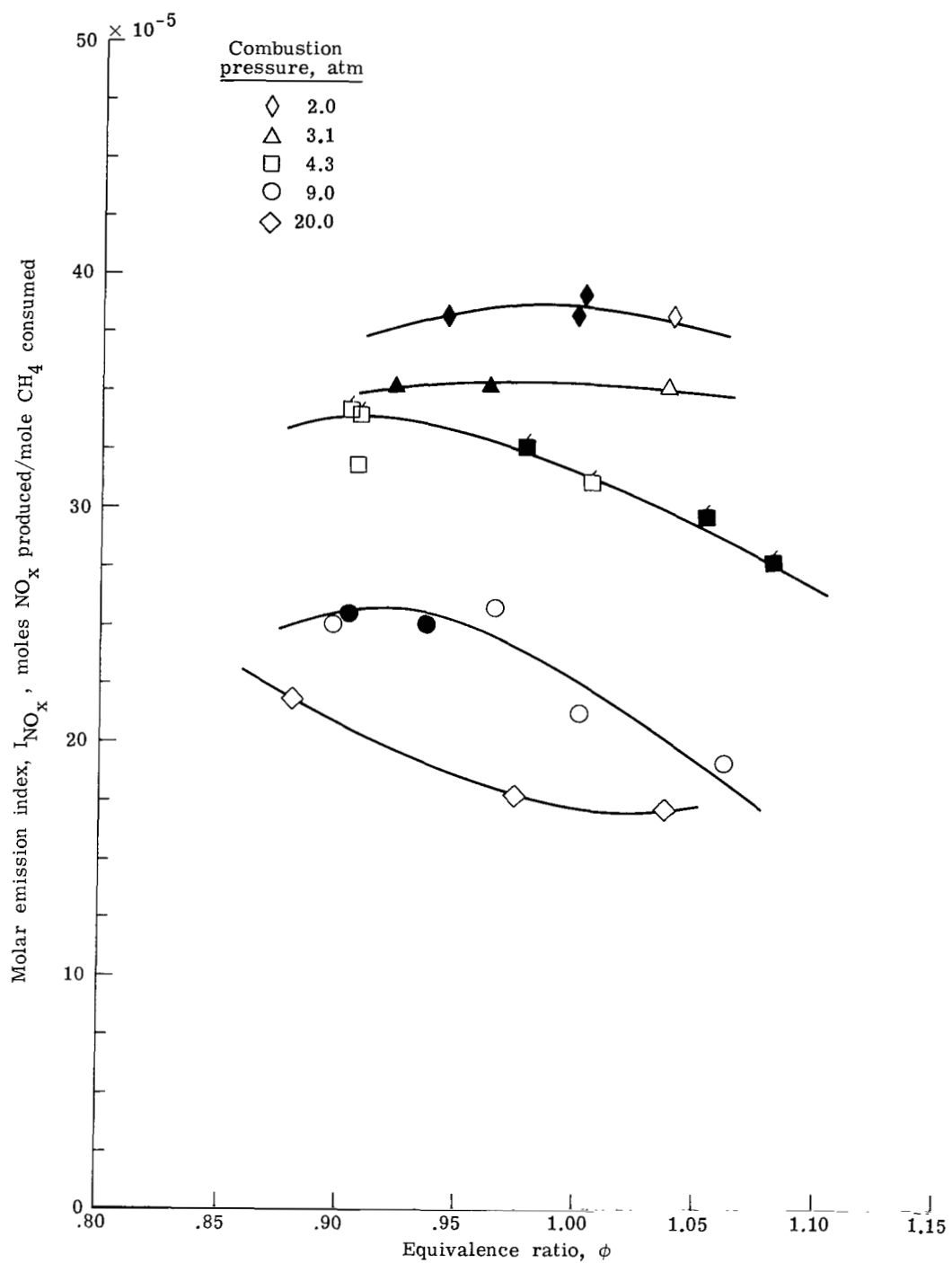
(c) Flameholder 4.

Figure 3.- Concluded.



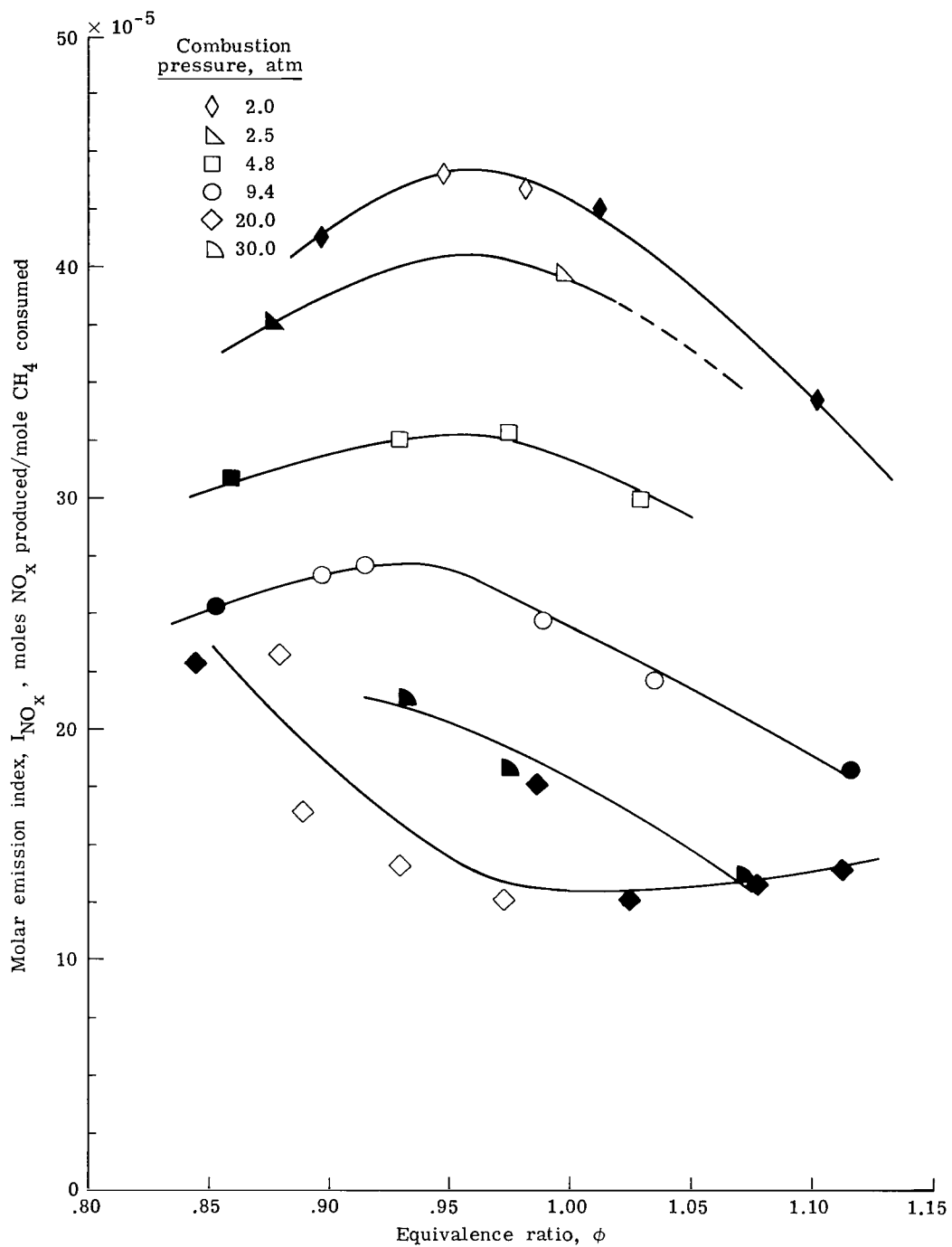
(a) Flameholder 1.

Figure 4.- Molar emission index of  $NO_x$  as function of pressure and equivalence ratio. Solid symbols: unstable flame.



(b) Flameholders 2 (marked with flag) and 3.

Figure 4.- Continued.



(c) Flameholder 4.

Figure 4.- Concluded.

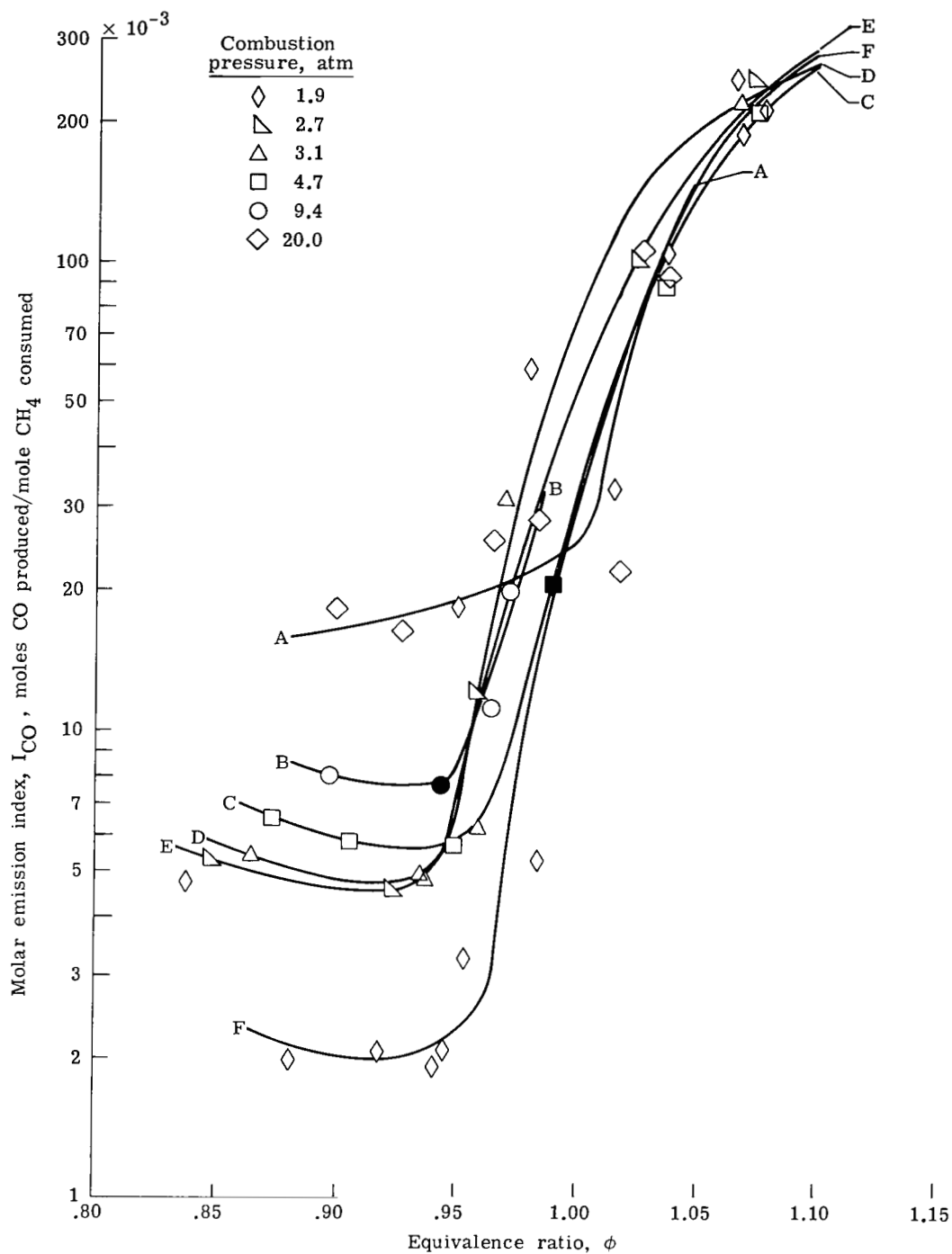
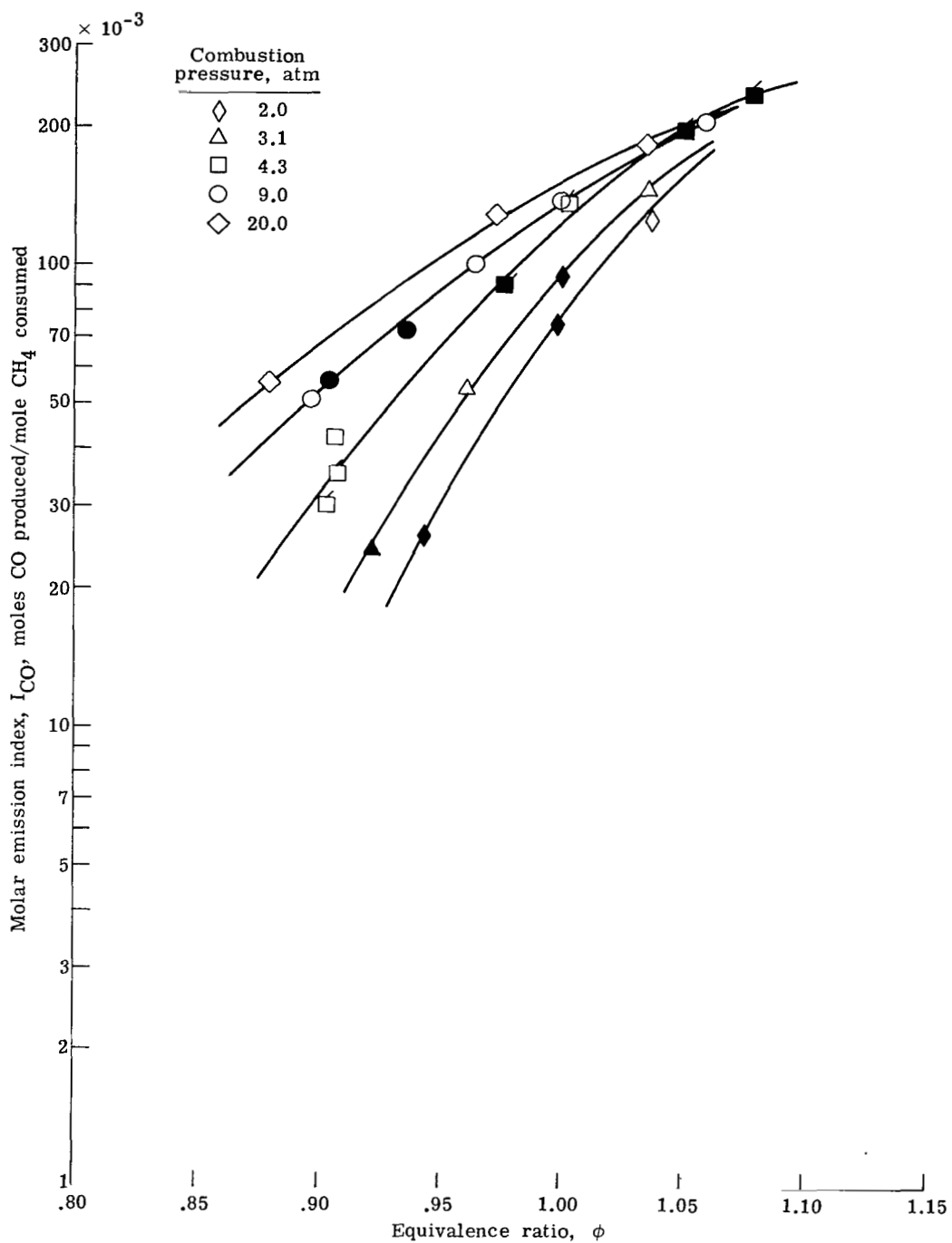


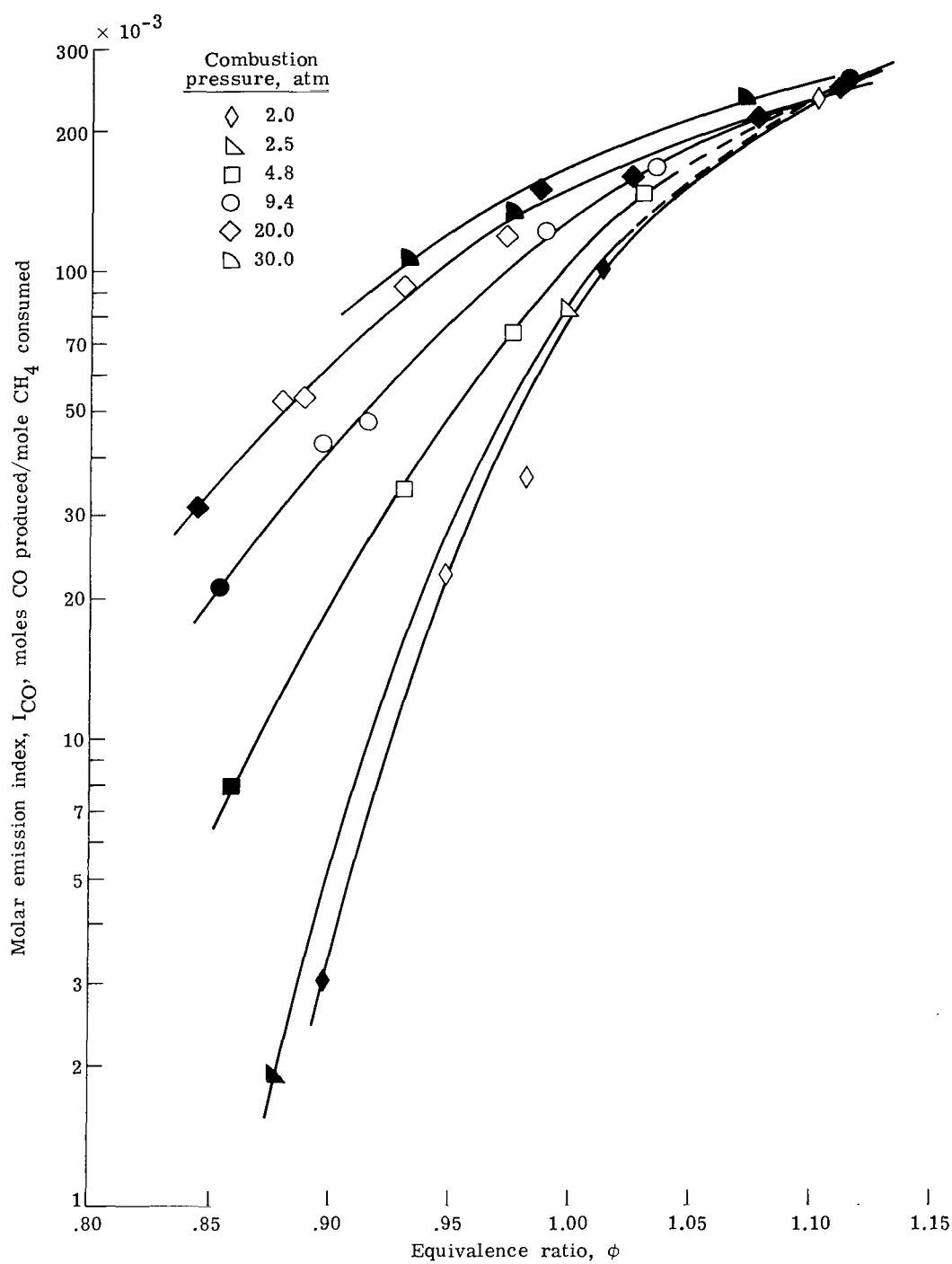
Figure 5.- Molar emission index of CO as function of pressure and equivalence ratio. Solid symbols: unstable flame.





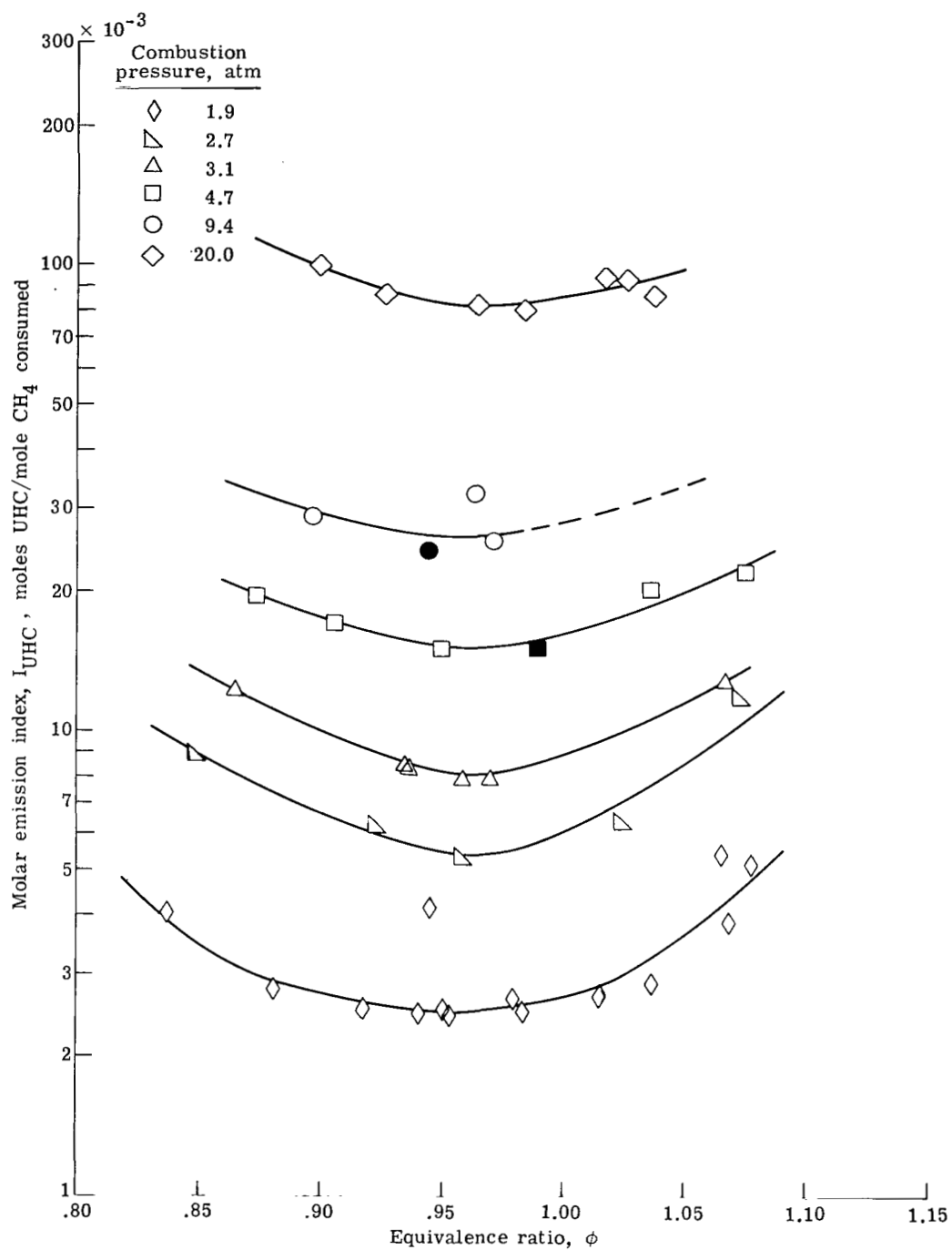
(b) Flameholders 2 (marked with flag) and 3.

Figure 5.- Continued.



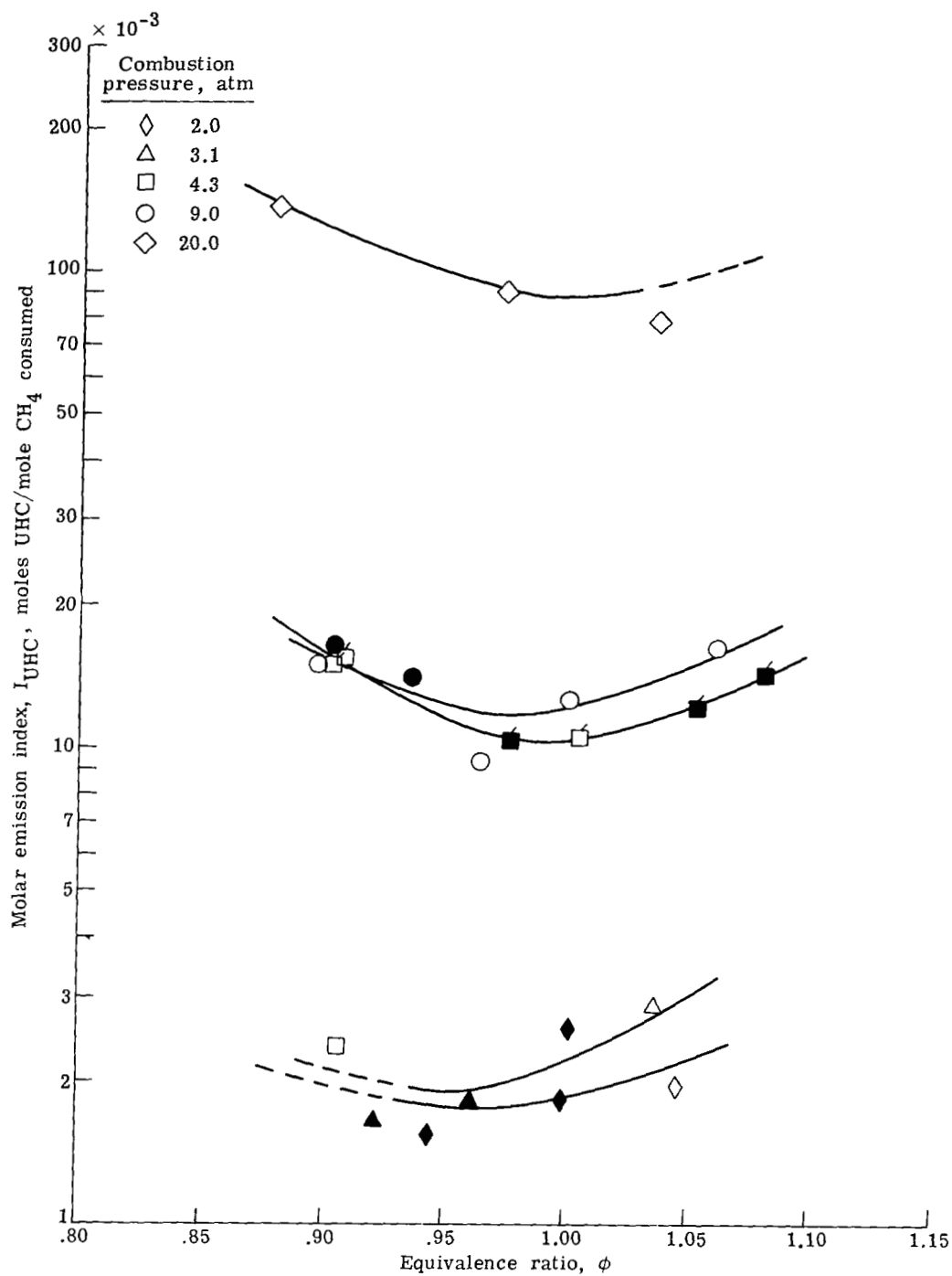
(c) Flameholder 4.

Figure 5.- Concluded.



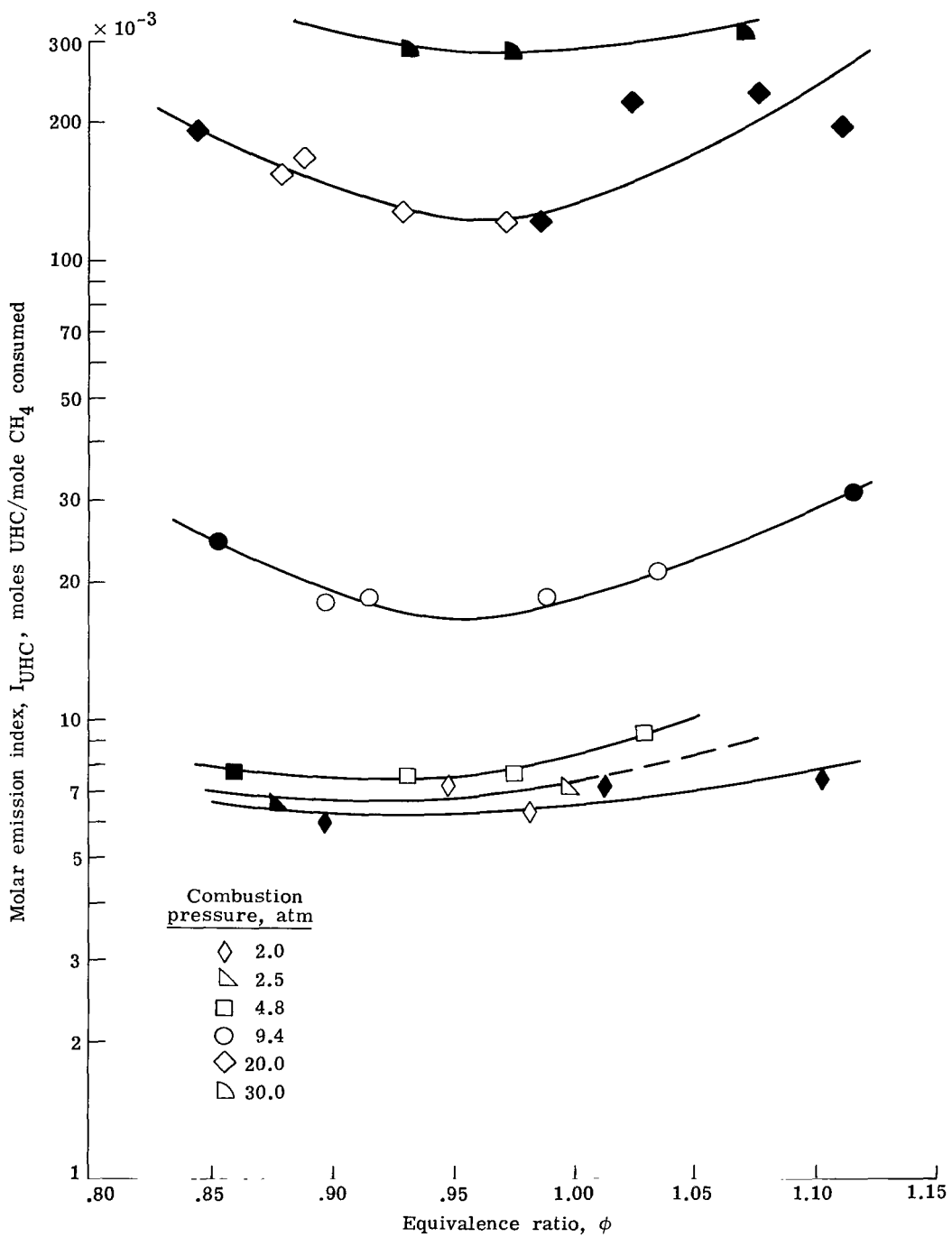
(a) Flameholder 1.

Figure 6.- Molar emission index of unburned hydrocarbons as function of pressure and equivalence ratio. Solid symbols: unstable flame.



(b) Flameholders 2 (marked with flag) and 3.

Figure 6. Continued.



(c) Flameholder 4.

Figure 6.- Concluded.

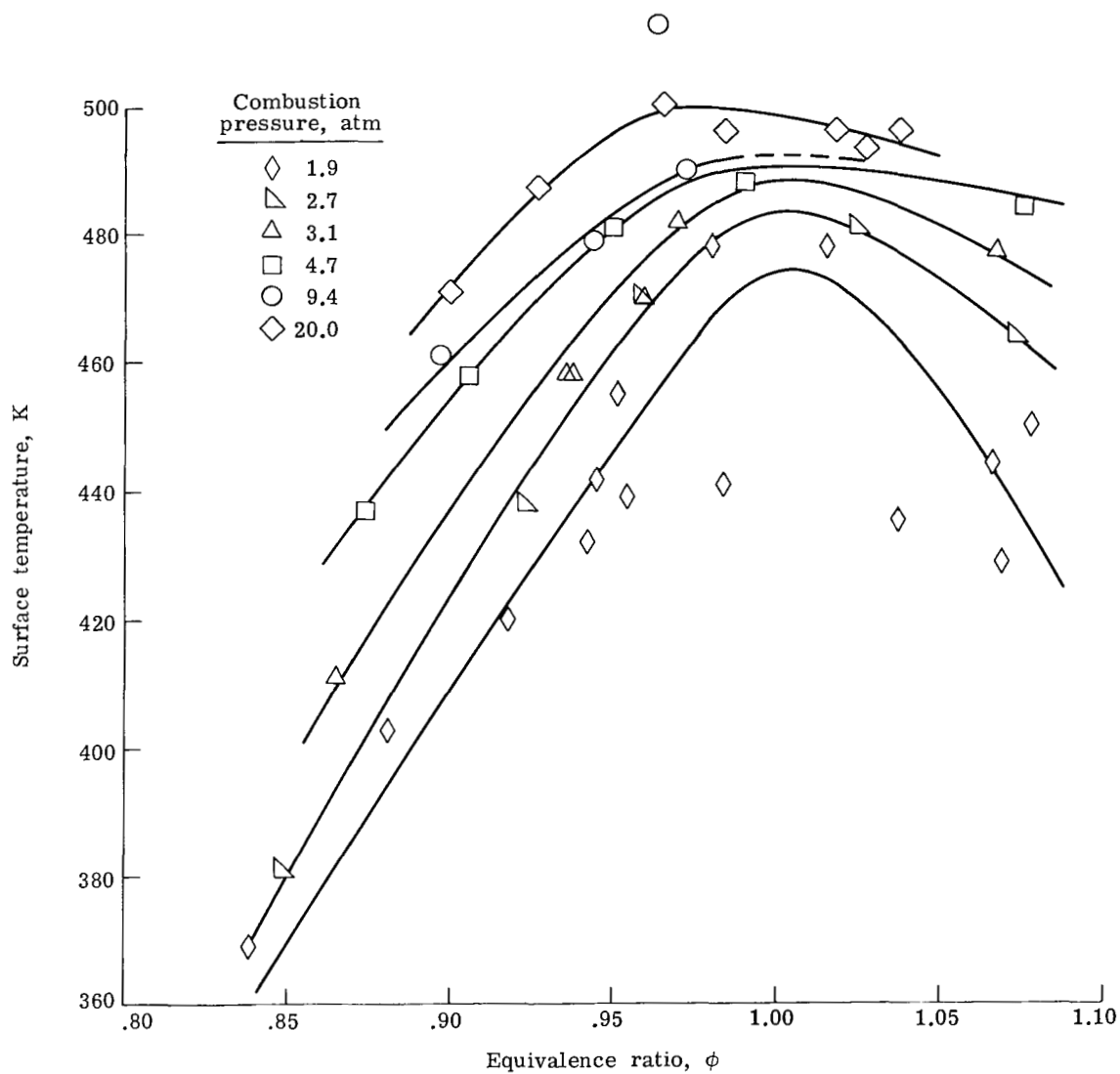


Figure 7.- Flameholder surface temperature as function of pressure and equivalence ratio. Flameholder 1.

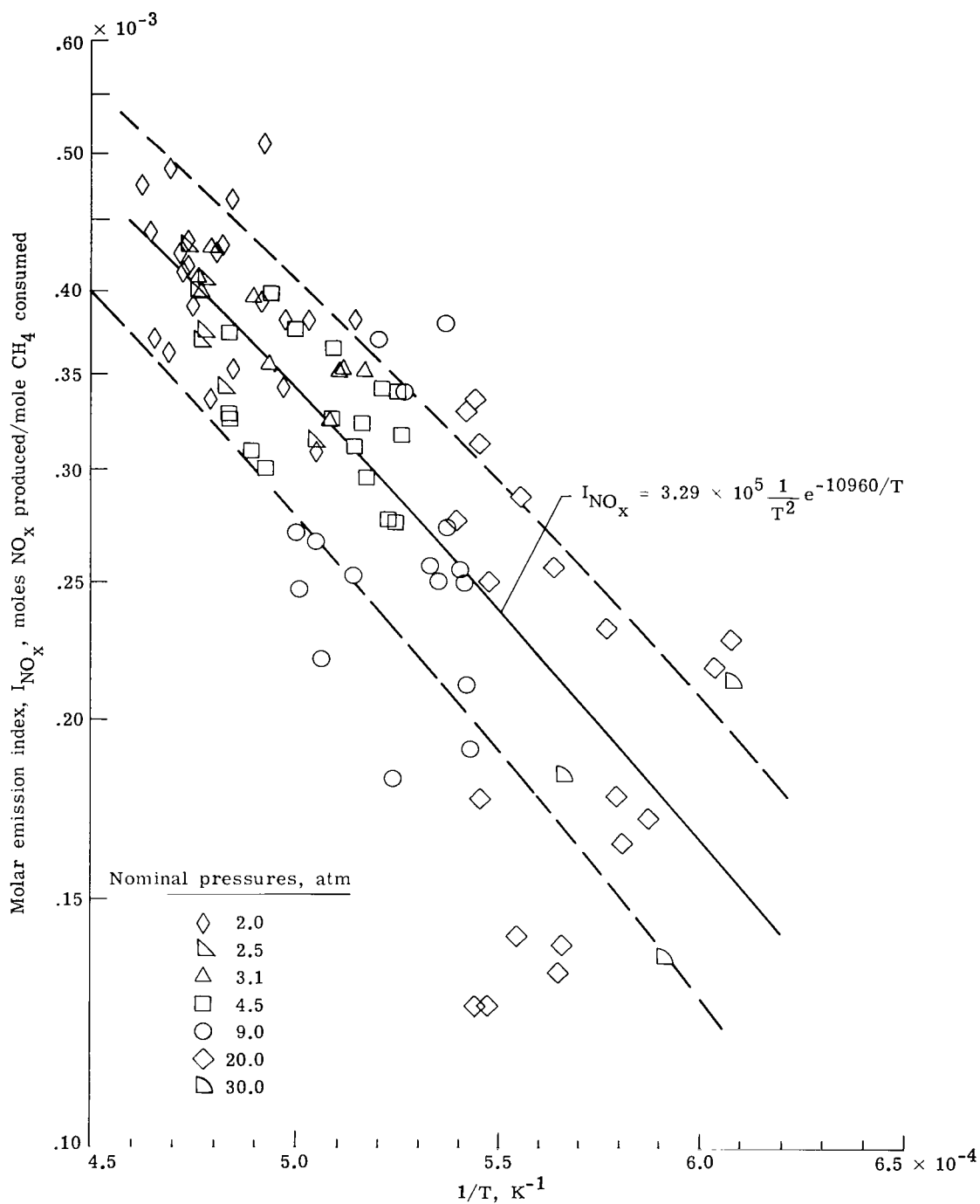


Figure 8.- Correlation of molar emission index for  $NO_x$  as function of inverse temperature. Data for all flameholders.

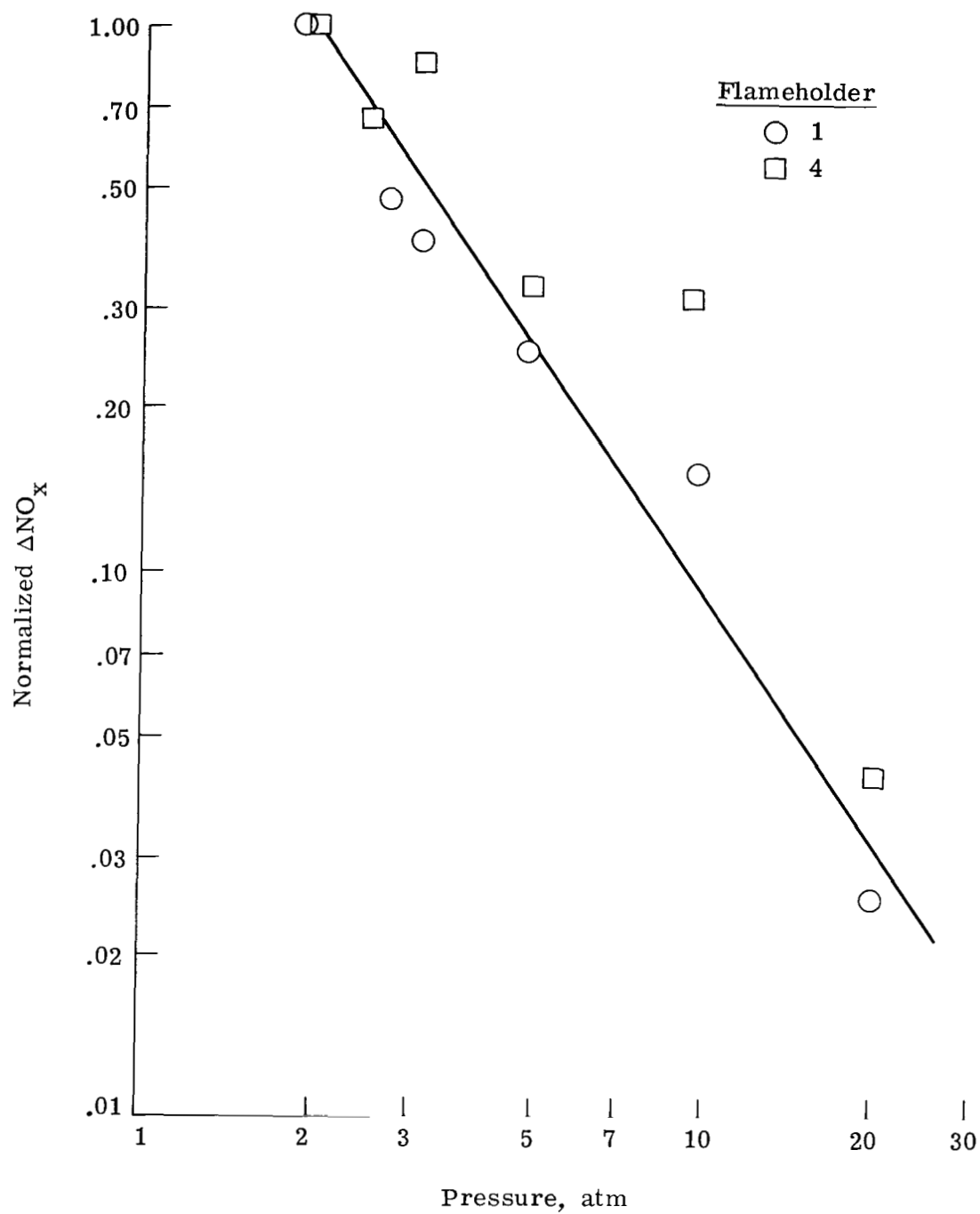


Figure 9.- Normalized change in concentration of  $NO_x$  produced by presence of thermocouple as function of pressure.



1. Report No. NASA TP-1673		2. Government Accession No.		3. Recipient's Catalog No.	
4. Title and Subtitle  POLLUTANT EMISSIONS FROM FLAT-FLAME BURNERS AT HIGH PRESSURES				5. Report Date June 1980	
				6. Performing Organization Code	
7. Author(s)  Howard G. Maahs and Irvin M. Miller				8. Performing Organization Report No. L-13550	
				10. Work Unit No. 146-20-10-07	
9. Performing Organization Name and Address  NASA Langley Research Center Hampton, VA 23665				11. Contract or Grant No.	
				13. Type of Report and Period Covered Technical Paper	
12. Sponsoring Agency Name and Address  National Aeronautics and Space Administration Washington, DC 20546				14. Sponsoring Agency Code	
15. Supplementary Notes					
16. Abstract <p>Maximum flame temperatures and pollutant emission measurements for NO<sub>x</sub>, CO, and UHC (unburned hydrocarbons) are reported for premixed methane-air flat flames at constant total mass flow rate over the pressure range from 1.9 to 30 atm and for equivalence ratios from 0.84 to 1.12. For any given pressure, maxima typically occur in both the temperature and NO<sub>x</sub>-emissions curves slightly to the lean side of stoichiometric conditions. The UHC emissions show minima at roughly the same equivalence ratios. The CO emissions, however, increase continually with increasing equivalence ratio. Flame temperature and NO<sub>x</sub> emissions decrease with increasing pressure, while the opposite is true for the CO and UHC emissions. The NO<sub>x</sub> data correlate reasonably well as a function of flame temperature only. Four flameholders, differing only slightly, were used in this study. In general, the temperature and emissions data from these four flameholders are similar, but some differences also exist. These differences appear to be related to minor variations in the condition of the flameholder surfaces.</p>					
17. Key Words (Suggested by Author(s)) Pollution Combustion High pressure Nitric oxide Premixed flame			18. Distribution Statement Unclassified - Unlimited  Subject Category 25		
19. Security Classif. (of this report) Unclassified		20. Security Classif. (of this page) Unclassified		21. No. of Pages 38	
				22. Price* \$4.50	

\* For sale by the National Technical Information Service, Springfield, Virginia 22161

NASA-Langley, 1980

National Aeronautics and  
Space Administration

Washington, D.C.  
20546

Official Business

Penalty for Private Use, \$300

THIRD-CLASS BULK RATE

Postage and Fees Paid  
National Aeronautics and  
Space Administration  
NASA-451



3 1 1U,C, 060280 S00903DS  
DEPT OF THE AIR FORCE  
AF WEAPONS LABORATORY  
ATTN: TECHNICAL LIBRARY (SUL)  
KIRTLAND AFB NM 87117

**NASA**

POSTMASTER: If Undeliverable (Section 158  
Postal Manual) Do Not Return

---